Mémoire

Auteur : Franckart, Axel
Promoteur(s) : Vandewalle, Nicolas
Faculté : Faculté des Sciences
Diplôme : Master en sciences physiques, à finalité approfondie
Année académique : 2023-2024
URI/URL : http://hdl.handle.net/2268.2/20415

University of Liège

Master Thesis presented in partial fulfilment of the requirements for the master degree in Physical Sciences

---

Array of spinners as a model for spin glasses

Axel Franckart

Promoter:
Prof. Nicolas VANDEWALLE

Reading committee:
Prof. Ngoc Duy NGUYEN
Prof. Peter SCHLAGHECK
Dr. Eric OPSOMER

Academic year 2023-2024

Acknowledgment

I want to express my gratitude to everyone who contributed to making this thesis possible.

First and foremost, I am thankful to my supervisor, Nicolas Vandewalle, for his guidance, insightful advice, and enthusiasm. I am also grateful to the members of GRASP and my classmates for their support and valuable advice. I would like to extend my acknowledgment to the members of the reading committee, Ngoc Du Nguyen, Peter Schlagheck, and Eric Opsomer, for taking the time to review my thesis. Finally, I want to thank Diogo Borges Soares and Nuno Araujo for their enthusiasm, wise counsel, and our productive monthly meetings.

Additionally, I am grateful to the Consortium des Équipements de Calcul Intensif (CÉCI) for providing the necessary computational resources, which were crucial for the numerical scientific computations involved in this research.

Abstract

With a ball bearing, three magnets, and a 3D printer, we have designed an experimental and macroscopic model of a magnetic spin called a "spinner," which behaves roughly like a dipole that can only rotate in a plane. Several spinners placed on a network can interact and create countless different configurations. If we are indeed dealing with a spin glass, these configurations will exhibit an ultrametric structure, analogous to a phylogenetic tree with a structure of meta-basins, basins, sub-basins, etc. The objective of this thesis will be to determine whether our device is indeed a spin glass. We will use numerical methods to explore the energy landscape and study the arrangement of stable configurations within it.

Abstract

Avec un roulement à billes, trois aimants et une imprimante 3D, nous avons conçu un modèle expérimental et macroscopique d'un spin magnetique appelé "spinner" se comportant grossièrement comme un dipôle ne pouvant tourner que dans un plan. Plsuieur spinners placées sur un réseaux peuvent interagir et créer d'innombrables configurations différentes. Si nous sommes effectivement en présence d'un verre de spinses, ces configurations présenteront une structure ultramétrique, c'est-à-dire analogue à un arbre phylogétique avec une structure en meta bassiin, bassin, sous bassins, etc. L'objectif de ce mémoire sera de déterminer si notre dispositif est bien un verre de spins. Nous allons utliser des moyens numériques pour exlorer le paysage énergétique et etudier la disposition des configuration stable dans celui-ci.

Contents

List of abbreviations

RSB	Replica symmetry breaking
SG	Spin glass
UM	Ultrametric
SUM	Subdominant ultrametric
GE	General energy
LE	Local energy
Ha	Hamming
IHa	Invariant Hamming

Part I

Introduction

What is the common point of the Great Barrier Reef's ecosystem, the brain of rats, and a social network? They are all composed of numerous components that interact with each other. Moreover, they have a lot of possible stable configurations: a species can take the place of one other, all brain regions are not simultaneously active, and we can change our friend circle in our media. A theoretical framework used to model the systems is called a Spin Glass (SG) [1–5]. Spin Glass theory takes root in magnetic materials. The paradigmatic model and definition of a SG is a set of magnets with fixed positions and without translation or rotational symmetry. The natural consequence of the absence of spatial symmetry is the increased complexity of the energetic landscape. Indeed, if we have translational symmetry and all magnets are similar, there is only one ground state, i.e. all magnets are aligned in one direction. It is the variation of pairwise interactions that brings about magnetic frustration and a rugged energetic landscape.

Spin glasses have been used as simple models to study glasses [6]: the magnets do not move, and the pairwise interactions are time-independent. The questions that arise include [6, 7]: What is the shape of the energetic landscape? Is there symmetry breaking during the glass transition? What is the temperature dependence of ergodicity? A picture of SG was provided by Parisi at his Physics Nobel Laureate lecture in 2021 [8]. At high temperatures, a spin glass behaves like a liquid, with thermal energy high enough to overcome all barriers in the energetic landscape. When we cool the spin glass, the highest energy barriers become difficult to pass, and ergodicity is broken, confining the system to a subregion of the configuration space. If we cool it further, lower barriers become difficult to pass, and ergodicity is restricted to a sub-subregion. This process can continue until the system reaches zero temperature. At a given temperature, the spin glass does not remain in one configuration but can wander arbitrarily far from it, exhibiting marginal stability [9]. An illustration of this can be seen in Figure 1.

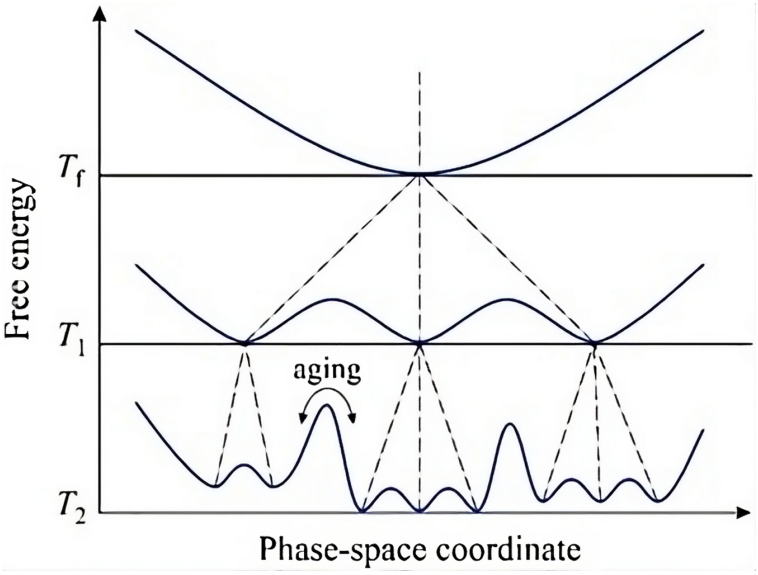

Figure 1: The energetic landscape changes as a function of temperature. When T decreases, the energetic minima split into additional minima. Furthermore, we can observe the beginning of a hierarchical structure in the energetic landscape [10].

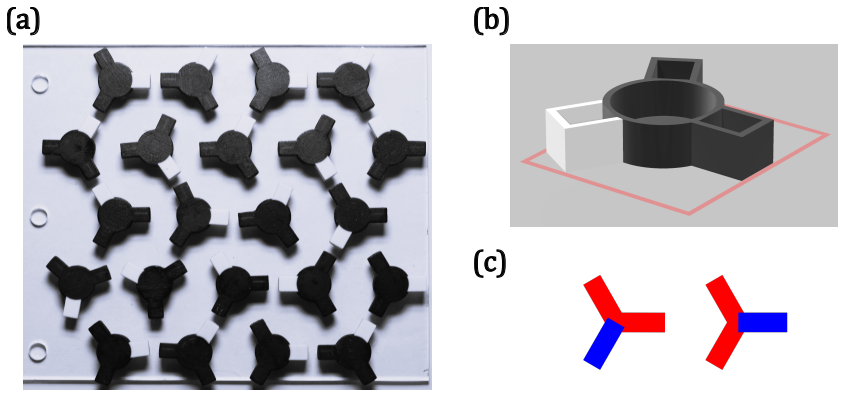

Figure 2: **(All)** The experimental model is composed of spinners that are simply dipoles embedded in a 3D-printed star that can rotate on a ball bearing. The colour code, black-white or red-blue, corresponds to inner or outer magnetic dipoles. **(a)** Experimental array of spinners. **(b)** 3D-printed object that will contain the three dipoles. **(c)** Schematic representation of two spinners.

Spin glasses are therefore characterized by a hierarchical structure in the energetic landscape [6], which is called ultrametric. This means there is an ordered arrangement of energy minima in the configurational space, similar to a phylogenetic tree, the minima can be grouped into species, genus, and family. We will use the terms sub-basin, basin, and meta-basin to describe these groupings. Ultrametric structures have been found in the structure of memory [11], the structure of DNA [12], as well as in spin glasses [13] and granular materials [14].

Despite the numerous spin glass models and variations [6, 7], there is still no experimental setup that displays the characteristic features of a spin glass, such as frustration, a high number of metastable configurations, and an ultrametric hierarchy of these configurations.

In this thesis, we will propose an experimental model for spin glass based on magnets with only one rotational degree of freedom, so-called "spinners", arranged on a grid. The model can be seen in Figure 2. Specifically, we place three quasi-point magnetic dipoles on a 3D-printed structure that can rotate on a ball bearing. Two dipoles point outward, and one point inward. These spinners are placed on a plate around an axis of rotation. They can rotate and form complex structures. Furthermore, the array can be placed under an external magnetic field. The main idea is that the association of three dipoles can create sufficiently complex interactions between the spinners, leading to a complex energetic landscape with a large set of metastable states. The essential point is that the characteristic size of the spinners is of the same order of magnitude as the lattice parameter.

To study how closely the experimental model approximates a spin glass, we will follow several steps. First, in Part II, we will introduce the main theoretical models of spin glass, the theoretical framework of replica symmetry in which this thesis will operate, and the notions of annealing and distance. Secondly, in Part III, we will develop an appropriate theoretical spin glass-like model for the device, guided by experimental observations and condensed matter analogies. Furthermore, we will verify and study the dependence of the number of metastable configurations and their ultrametric or non-ultrametric behaviour as a function of the lattice parameter, the number of spinners, and the external magnetic field. This will allow us to answer the fundamental question: is an array of spinners a spin glass? Additionally, we will gain initial insights into the physics of the system and the structure of the configurational space.

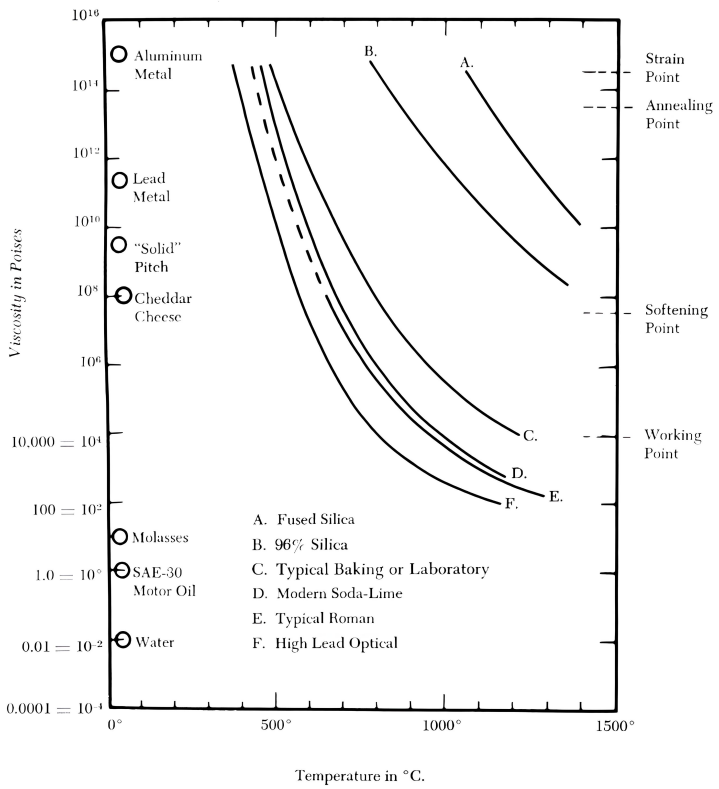

Figure 3: T-dependence of viscosity for a range of glass and glass-forming liquid [15].

Part II

State of the art

1 Glass

A glass can be defined as a non-crystalline solid with a glass transition [15]. The first point is straightforward: "non-crystalline" means that there is no elementary cell and no translational symmetry; in other words, the solid is disordered. The second element is the glass transition: it is not a phase transition, but rather a process where some physical properties change radically below a critical temperature range, known as the glass transition temperature T_g [16–18]. The general recipe for making a glass involves taking a liquid and cooling it quickly enough so that thermal fluctuations are not sufficient to overcome the energetic barriers of crystallization, as seen in supercooled liquids [19]. As displayed in Figure 3, when we cool glass-forming liquids, the viscosity increases and diverges as the diffusion coefficient vanishes [20]. The particles no longer have sufficient thermal energy to move and change the structure of the glass. Specifically, below a critical temperature, the configurational entropy vanishes [21], the system falls into a given configuration, and the relaxation time to escape this configuration also diverges: it is a glass transition. The cooling rate and the chemical composition are the two main parameters that determine T_g. We say that the glass has fallen out of equilibrium. Although a liquid lacks symmetry, it is in an equilibrium state because particles can gain energy through collisions due to thermal energy, but their energy is dissipated by viscosity [22]. Both

phenomena occur on the same time scale. The main point is that when a glass-forming liquid is cooled, the viscosity diverges, causing the time scale of diffusion processes to become much greater than that of thermal oscillations by several orders of magnitude [22, 23]. The liquid is lost in a restricted region of its phase space and the ergodicity is lost [24]. Research on glass is important due to its industrial and economic significance, particularly for applications such as optical fibers and windows. In the following section, we will present SG model with an analogous behaviour that glass.

2 Spin glass

The concept of Spin Glass (SG) was introduced by Anderson in 1970 to study the dilution of magnetic metals in non-magnetic metals [25]. Analogous to the concept of glass, a spin glass is a disordered system where each vertex of a graph can have a spin. There is no translational symmetry, so the coupling is different for each pair of spins. This concept also serves as a model for discrete granular materials and real glass [7]. A spin glass, like traditional glass, exhibits an analog of the glass transition: below a critical temperature, the relaxation time diverges, and the system falls out of equilibrium.

Two major parts of SG literature will catch our attention. First, we will investigate some famous models that have attempted to describe this transition out of equilibrium into a frozen state. Secondly, we will explain the replica symmetry breaking developed by Parisi. Finally, this will give us the tools to describe our experimental system as a SG and to study its energetic landscape.

2.1 Ising model

The Ising model is a renowned model used to describe the transition between ferromagnetism and paramagnetism [26, 27]. It is one of the simplest and earliest models (1925) to describe this transition.

2.1.1 Definition

Let us examine a set of N Ising spins denoted as $\{S_i\}_{i=1,\dots,N}$, where each spin can assume a binary value $S_i = \pm 1$. These spins are placed on a periodical lattice. The interactions between spins are governed by the exchange coupling constant J, being the interaction strength between neighbouring spins S_i and S_j. In addition, the spins can interact also with an external magnetic field B. For a given spin configuration $\underline{S} = \{S_i\}$, the energy of this system is described by the corresponding Hamiltonian defined as follows:

$$H[\underline{S}] = -J \sum_{\langle ij \rangle} S_i S_j - \sum_i B_i S_i, \tag{2.1}$$

where the summation in the Hamiltonian is over the first neighbors only. Additionally, the system is subject to an external magnetic field, denoted by B_i, representing the magnetic field value at the site of spin S_i.

At first glance, we can deduce from the Hamiltonian expression that configurations minimizing the energy exhibit ferromagnetic order when $J > 0$, indicating a preference for aligned spins. This behavior is depicted in Figure 4 (a). Conversely, for $J < 0$, the system tends towards an antiferromagnetic order. Similarly, an alignment between spins and the magnetic field is the most energetically favourable configuration.

With statistical tools, we can infer the behavior of a lattice of Ising spins. First, the probability of observing a specific configuration $\underline{S}$ is governed by the Gibbs-Boltzmann distribution [6]

$$P_{GB}[\underline{S}] = \frac{e^{-\beta H[\underline{S}]}}{Z}, \tag{2.2}$$

where the partition function Z is defined as $Z = \sum_{\underline{S}} e^{-\beta H[\underline{S}]}$, within the canonical ensemble framework. Here, $\beta = 1/k_B T$ represents the inverse of the product of temperature T and the Boltzmann constant k_B.

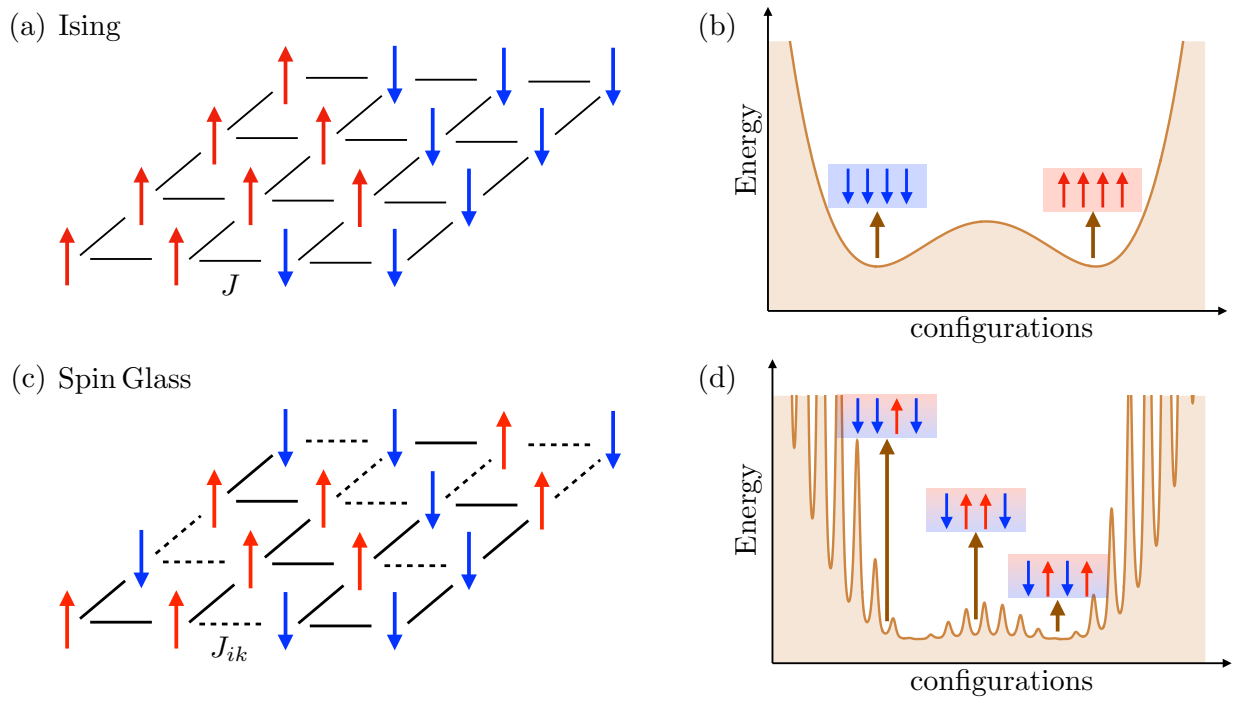

Figure 4: **(a)** Illustration of the Ising model: all spins have the same coupling term, and the order depends only on the sign of J: ferromagnetic if $J > 0$ and antiferromagnetic otherwise. **(b)** Illustrative plot of the energetic landscape. The Ising model has only two stable states, corresponding to all spins aligned in the same direction (up or down). If $J > 0$. The natural order parameter is magnetization. **(c)** Unlike the Ising model, here we have a coupling interaction J_{ik} that depends on each pair of spins. This distribution of J_{ik} is fixed for one system and can be seen as a random variable that parametrizes physical observables. This distribution will limit the length of ferromagnetic domains and lead to many metastable states characterizing the SG phase. **(d)** The energetic landscape of a SG has an infinite number of local minima in the thermodynamic limit; the challenge is its characterization.

Now we are able to compute the free energy

$$F = -k_B T \ln Z. \tag{2.3}$$

With the knowledge of F, the statistical average of any physical observable denoted by $\langle \bullet \rangle$, can be computed. Typical examples are energy average U and entropy S [6] :

$$U = \langle H[\underline{S}] \rangle = \frac{\partial(\beta F)}{\partial \beta}, \tag{2.4}$$

$$S = \langle -k_b \log P_{GB}[\underline{S}] \rangle = \frac{U - F}{T}. \tag{2.5}$$

The interest of the Ising model lies in its solvability in one and two dimensions, which will be the subject of the following sections.

2.1.2 One-dimensional solution

The one-dimensional Ising model was solved by Ising in 1925 [26]. Let's consider a chain of N spins with a coupling strength J that obeys the Hamiltonian given by Eq.(2.1) without the magnetic term. The boundary conditions of the model are periodic, which means $S_{N+1} = S_1$. In that case, Ising demonstrated that the partition function has the following expression [26, 27]

$$Z = 2(2\cosh \beta J)^{N-1}. \tag{2.6}$$

This expression helps us determine the likelihood of spin alignment at distance j, which is given by

$$\langle S_i S_{i+j} \rangle = (\tanh \beta J)^j = \exp\left(-j/\xi\right). \tag{2.7}$$

This indicates that spin alignment depends only on the temperature T and the coupling constant J. If the coupling constant is strong and positive, alignment is more likely. In addition, we have $|\langle S_j S_{j+1} \rangle|$ is stricly majored by 1 for any value J and for $T > 0$. The important consequence is that the likelihood of spin alignment between two spins decreases exponentially with the distance between them. This implies that alignment can not occur for a sufficiently significant N. In fact, any correlation length $\xi = (\ln \tanh \beta J)^{-1}$ will be small in comparison with the growing length of the spin chain. In one dimension with a first neighbour interaction, a phase transition is therefore impossible.

If we consider a uniform magnetic field, i.e. $B_i = B$. Using a transfer matrix method, Ising showed that the partition function has the following expression [26, 27]

$$Z = \lambda_+^N + \lambda_-^N, \tag{2.8}$$

where

$$\lambda_\pm = e^{\beta J}\left[\cosh \beta B \pm \sqrt{\cosh^2 \beta B - 2e^{-\beta J}\sinh 2\beta J}\right]. \tag{2.9}$$

From this, we can derive the magnetization of the chain, i.e.

$$M(B,T) = \frac{e^{\beta J}\sinh \beta B}{\sqrt{e^{2\beta J}\sinh^2 \beta B + e^{-2\beta J}}}. \tag{2.10}$$

This means that, despite the presence of a magnetic field B, there is no spontaneous magnetization, and the system does not undergo a transition between ferromagnetism and paramagnetism.

Nevertheless, a transition could happen if the interactions have long-range effects. In fact, an interaction that scales as $r^{-\sigma}$, where r is the distance between interacting spins, can induce a transition only if $1 < \sigma \leq 2$ [28]. If $\sigma > 2$, the system becomes disordered, lost somewhere in its configurational space. The decrease rate of this interaction is a determinant element in the behaviour of a spin chain. For an array of spinners, the decay of the interaction will be an interesting question because that can influence the degree of order and the glassy behaviour.

2.1.3 Two-dimensional solution

The two-dimensional Ising model, without an external magnetic field B, was solved by Onsager in 1943 [29]. The remarkable result is the analytical value for the critical temperature T_c of the second-order phase transition between ferromagnetic order below T_c and paramagnetic order above T_c. One has

$$T_c = \frac{J}{k_b \ln\left(1+\sqrt{2}\right)} \tag{2.11}$$

In addition, Onsager determined the extrapolation of the mean correlation length [29]

$$\xi = (\exp 2\beta J \tanh 2\beta J)^N, \tag{2.12}$$

which is an increasing function concerning N and decreasing concerning T. The correlation length is an important characteristic of disordered systems, serving as a measure of local order. Specifically, it provides information on the characteristics of ferromagnetic domains. In, addition it tells us that the intensity of the interaction between two spinners can influence the correlation length.

2.2 Experimental spin glass

In the second half of the twentieth century, condensed matter physicists began studying magnetic impurities in metals, such as Mn in Cu, see Figure 5 (a) [30]. They observed strange phenomena, such as a cusp in magnetic susceptibility but no cusp in the specific heat [31]. This indicates the presence of a phase transition that is not a classical one [32]. Additionally, they observed a minimum in the resistivity $\rho(T)$ at low temperatures, known as the Kondo effect [33]. The presence of impurities breaks the translational symmetry, making it challenging to develop a theory for this experimental Spin Glass (SG) system.

Moreover, magnetic impurities can interact with each other through the Ruderman-Kittel-Kasuya-Yosida (RKKY) interaction [30, 34] with a potential

$$V(r) = \frac{\cos 2k_F r}{r^3}, \tag{2.13}$$

where k_F is the Fermi wave vector, and r is the distance between two impurities. The cosine term is crucial because it allows the interaction to be either ferromagnetic or antiferromagnetic. This element plays a central role in describing the Edwards and Anderson model, as discussed in Section 2.3, as it induces frustration being a major ingredient of SG.

In summary, dilution introduces randomness to the system, and the RKKY interaction contributes to frustration due to its varying signs. These are the two typical characteristics of SG phases. The consequence of the complexity and randomness of microscopic structure is that it is difficult to measure or model the structure and behaviour of glass. That is important and has stimulated the development of a more complex model, than the Ising model, characterized by a no constant interaction term. This model is discussed in Section 2.3 and 2.4.

2.3 Edwards-Anderson model

In 1975, Edward and Anderson proposed a model [35] to describe the behaviour of a dilution of Mn in Cu [30, 31], as discussed in Section 2.2. Like the Ising model, N spins are considered on a periodic lattice, but they are randomly placed. It is a random graph, as shown in Figure 5 (a). The system is described by the Hamiltonian

$$H_{\mathcal{J}}[\underline{S}] = -\frac{1}{2}\sum_{ij} J_{ij} S_i S_j. \tag{2.14}$$

The summation encompasses all spins, implying an infinite-range interaction model where every spin i interacts with every other spin j. This interaction is not only symmetrical, i.e. $J_{ij} = J_{ji}$, but also excludes self-interaction, ensuring $J_{ii} = 0$. Furthermore, the Hamiltonian depends on a random variable $\mathcal{J}$ that determines the distribution of J_{ij}, which can follow any distribution, not solely a Gaussian one. This characteristic is called quenched disorder because the spins are frustrated by the random and anisotropic interactions. In addition, the spins are not allowed to move, so the coupling J_{ij} cannot change. The distribution of J_{ij} determines the behavior and the scale of ferromagnetic and antiferromagnetic domains. Consequently, at low temperatures, the spin system is blocked in a metastable state different from the lowest energy state. If the temperature is low enough, the relaxation time to pass the energetic barrier that blocks the system in this state diverges. This is a spin glass state.

The transition between ferromagnetism and paramagnetism can be observed through the magnetization. In other words, the free energy F can be expressed as a function of magnetization only, with temperature as a parameter. Under T_c, F looks like Figure 4 (b). In the Edwards-Anderson model, there is a transition between the SG state and paramagnetism at a critical temperature T_c^{SG}, as illustrated in Figure 5 (b), when the thermal energy k_bT is more important that the variance of the interaction term $\tilde{J}$. The theoretical critical point is given by

$$k_b T_c^{SG} = \sqrt{\sum_{ij} \langle \tfrac{2}{9} J_{ij}^2 \epsilon_{ij} \rangle}, \tag{2.15}$$

where ϵ_{ij} is 1 if sites i and j are occupied by a spin, and 0 otherwise. Similar to the results of the 2D Ising model, as shown in Eq.(2.11), the critical temperature exhibits analogous behaviour. However, the free energy F now looks as depicted in Figure 4 (d). Consequently, many metastable states can have the same magnetization, and ferromagnetic long-range domains could not happen, and as a consequence, magnetization cannot be an order parameter for the SG transition. The fundamental question is: which symmetry is breaking in the SG phase?

At low temperatures, we expect that spins do not flip so much, so the local magnetization will not be zero, i.e., $\langle S_i \rangle \neq 0$. However, the system depends on a random variable $\mathcal{J}$, so we need to study an *ensemble* of versions of the system, one for each value of $\mathcal{J}$ [8]. The local magnetization is not a relevant order parameter because it is a function of $\mathcal{J}$. Edward and Anderson had the idea to introduce an order parameter q_{EA} that quantifies the spin-flip symmetry:

$$q_{EA} = \frac{1}{N} \sum_i |\langle S_i \rangle|^2. \tag{2.16}$$

At temperatures above T_c^{SG}, the order parameter q_{EA} is zero, meaning a paramagnetic phase where spin flips lead to the vanishing of dynamical averages. Conversely, below T_c^{SG}, when $q_{EA} \neq 0$, the phase corresponds to a SG, indicating that the quantity of spin flips decreases until disappearing at $T = 0$ and, the magnetic order appear [8].

The challenge is to compute an average of thermodynamic observables over $\mathcal{J}$, denoted by $\overline{\bullet}$, which is the so-called solved spin glass model [34]. This average can be computed using [8] the so-called replica trick. Following this mathematical trick, one can compute the average partition function

$$\overline{F} = -Tk_B \overline{\ln Z_{\mathcal{J}}} = -Tk_B \lim_{n \to 0} \frac{\overline{Z_{\mathcal{J}}^n - 1}}{n}. \tag{2.17}$$

Instead of calculating $\overline{\ln Z_{\mathcal{J}}}$, we can focus on computing the average of $\overline{Z_{\mathcal{J}}^n}$, where $n \in \mathbb{N}$. This is often more straightforward. $Z_{\mathcal{J}}^n$ can be interpreted as the partition function of nN spins. Instead of considering a single system, we examine n replicas of the system. All replicas have the same $\mathcal{J}$; they are coupled after averaging the free energy. This interpretation is not rigorously justified because taking the limit $n \to 0$ involves non-integer values of n, which does not make physical sense [8, 30, 34, 36]. Edwards and Anderson proposed a

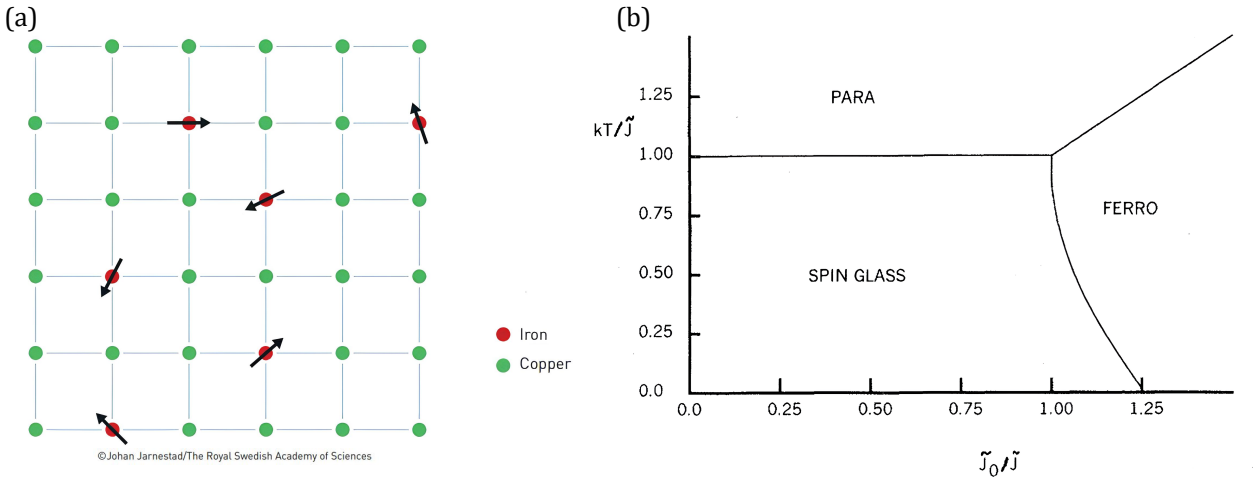

Figure 5: **(a)** In this schematic representation, we illustrate the dilution of iron in copper. The iron nuclei occupy a fraction of all atomic sites, and their positions are randomly distributed. Since iron is magnetic while copper is not, this physical system can be conceptualized as a randomly spatially distributed interacting spin system, serving as inspiration for the Edwards and Anderson model [35]. **(b)** Phase diagram by Sherrington and Kirkpatrick [37], as a function of a measure of the importance of fluctuations in the interacting coupling $\tilde{J}_0/\tilde{J}$ (lower values indicate significant fluctuations) and a measure of the dominance of thermal energy over the interaction coupling between spins $kT/\tilde{J}$. The diagram delineates three phases: paramagnetic if thermal energy dominates, ferromagnetic if the mean interaction coupling dominates, and frozen if coupling fluctuations dominate. This last phase corresponds to a spin glass phase.

generalized order parameter that could parameterize the average free energy, based on a generalization of q_{EA},

$$q_{\alpha\beta} = \frac{1}{N}\sum_i S_i^\alpha \cdot S_i^\beta. \tag{2.18}$$

Here, α and β represent two replicas of the system, and when both are equal, we have $q_{\alpha\alpha} = q_{EA}$. This order parameter quantifies a difference, a symmetry, between replicas. It marks the first instance where an order parameter dependent on more i.e. one configuration has been considered.

The Edward-Anderson model has given us a way to treat anisotropy in a spin glass and that will be used in Section 3.2 for the array of spinners. Plus, we have introduced the concept of replica symmetry that is fundamental in SG theory, see Section 2.5, and that we will be used to study many configurations of the same array of spinners. The following section will present an amended Edawrd-Anderson model that can be solved, i.e. the average free energy can be computed.

2.4 Sherrington-Kirkpatrick solvable model

Sherrington and Kirkpatrick proposed a simplification of the Edwards-Anderson model, assuming that interactions are of infinite range with a Gaussian distribution [37]. One has

$$P(J_{ij}) = \frac{e^{-(J_{ij}-J_0)^2/2J^2}}{\sqrt{2\pi}J}, \tag{2.19}$$

where J_0 and J are respectively the mean and the standard deviation of the distribution. Additionally, we choose the scaling $J_0 \sim N^{-1}$ and $J \sim N^{-1/2}$. All of these assumptions and simplifications aim to create a

solvable model, meaning a model where the average free energy can be computed analytically. We have

$$\overline{Z_{\mathcal{J}}^n} = \int dQ \exp\big(-N\beta\overline{f_n}(Q)\big) \approx \exp\big(-N\beta\overline{f_n}(Q_n^*)\big) \tag{2.20}$$

where $\overline{f_n} = \lim_{N\to\infty} \overline{F}/N$ is the average free energy per spin in the thermodynamic limit. Q is an $n \times n$ real symmetric matrix with null diagonal elements. Additionally, Q_n^* is a matrix derived from Q for which $f_n(Q_n^*)$ is a local minimum. The form of this matrix is a complex question that has involved a lot of theoretical development and encountered challenges [8]. This will be discussed in Section 2.5. Sherrington and Kirkpatrick deduce from their model a phase diagram, illustrated in Figure 5. The SG phase is characterized by a small thermal energy compared to the standard deviation of the coupling terms and a large standard deviation compared to the mean coupling term, indicating frustration. The following section will present an amended Edawrd-Anderson model that can be solved, i.e. the average free energy can be computed.

2.5 Replica symmetry breaking

The transition to the SG phase from the paramagnetic phase occurs as the temperature decreases, and the system jumps from one stable configuration to an infinite number of other stable configurations. In the classical transition from ferromagnetism to paramagnetism, symmetry is broken, leading to distinct magnetization values on either side. However, during the SG transition, the question arises: which symmetry is broken? The answer is related to the concept of phase coexistence. A transition between two phases is characterized by an observable $\mathcal{O}$ that takes on distinct values in both phases, such as magnetization for ferromagnetic transitions or density for liquid-gas transitions. At the transition, we have to add to the Hamiltonian a term that depends on this observable, coupled with a parameter ϵ [6]. One has

$$\Delta H = -\epsilon \int \mathcal{O}(\mathbf{x}) d\mathbf{x}. \tag{2.21}$$

We effectively have a phase coexistence if $\lim_{\epsilon\to 0^+}\langle\mathcal{O}\rangle \neq \lim_{\epsilon\to 0^-}\langle\mathcal{O}\rangle$. The question remains: what is the observable for a glass transition? It needs to have a different value for each possible phase. When a liquid is cooled, there are many ways it can crystallize, an infinity of possibilities that differ only by translation or rotation [6]. The game-changing idea has been proposed again by Edward and Anderson [35]. We need to consider a Hamiltonian of many replicas of the system, for example, two replicas denoted by α and β. This Hamiltonian is given by

$$H(\alpha,\beta) = H(\alpha) + H(\beta) + \epsilon d(\alpha,\beta), \tag{2.22}$$

where the observable d is a distance between both replicas, as defined by

$$d(\alpha,\beta) = \frac{1}{N} \min_{\mathcal{P}\in P_N} \sum_{i=1}^{N} |S_i^\alpha - S_{\mathcal{P}(i)}^\beta|^2. \tag{2.23}$$

This distance computes the mean square displacement between the two replicas with an all minimization over spin permutations $\mathcal{P}$. The Hamiltonian $H(\alpha,\beta)$ exhibits phase coexistence at $\epsilon = 0$. If we tend to $\epsilon \to 0^+$, to minimize H, we must minimize the distance d between replicas. As it vanishes at zero temperature, it means that the replicas need to be equal. Conversely, if we tend towards $\epsilon \to 0^-$, the distance d must increase significantly to minimize H. This formulation introduces the concept of Replica Symmetry Breaking (RSB), signifying that replicas are not identical but display certain symmetry breaking below a critical parameter. The natural order parameter is the likelihood of finding a given distance d, denoted as $P(d)$. If it is a delta function as in a liquid phase, we have replica symmetry; otherwise, we have replica symmetry breaking as in a crystal phase. Note that Eq. (2.22) corresponds to a thought experiment on the coexistence of two crystalline phases, α and β. A distance can be an appropriate observable to distinguish the replica symmetry phase from the RSB phase, similar to how magnetization distinguishes between ferromagnetic and paramagnetic phases.

A liquid-cooled can form an infinity of different glasses, so we need an infinity of different replicas. All of these are characterized by a probability of occurrence ω_α. The SG phase transition point can be seen as an infinite phase coexistence. Below this point, the system belongs to a specific phase. The Gibbs phase rule implies that we need *n-1* parameters if we have the coexistence of n phases. All of this relates to the formulation of the matrix Q, as seen in Eq.(2.20) [30, 34, 36]. Indeed, Parisi has found the form of the matrix Q that minimizes $\overline{f_n(Q)}$, as shown in Figure 6. It is an $n \times n$ matrix. First, we are interested in the sub-matrix q of Q, with the size $s = n - 1$. If we have replica symmetry, the form of q is given by

$$q_{\alpha\alpha} = q_d \qquad \text{and} \qquad q_{\alpha\neq\beta} = q, \tag{2.24}$$

where α and $\beta \in \{1, \ldots, s\}$. The matrix is invariant under permutation of replica groups, denoted by $\mathcal{P} \in P_s$, i.e. $q_{\alpha\beta} = q_{\mathcal{P}(\alpha)\mathcal{P}(\beta)}$. Parisi's idea of constructing q for a Replica Symmetry Breaking (RSB) is iterative; we start with a set of symmetric replicas, and then we have two sets, until, in the end, we have an infinite number of sets. The first set is one-step replica symmetry breaking (1RSB). We need an integer m_0 such that it divides s. We form s/m_0 subsets of replicas and label each subset as $l_\alpha^{(1)} \in 1, \ldots, s/m_0$, representing the subset of replica α formed during the first replica-breaking step. The matrix q look as [6]

$$q_{\alpha\beta} = \begin{cases} q_d & \text{if } \alpha = \beta \\ q_1 & \text{if } \alpha \neq \beta \text{ but } l_\alpha^{(1)} = l_\beta^{(1)} \\ q_0 & \text{if } l_\alpha^{(1)} \neq l_\beta^{(1)} \end{cases} \tag{2.25}$$

As illustrated in Figure 6, the matrix q has sub-blocks along the diagonal with values q_1, and the off-diagonal elements of the blocks are q_0. This procedure can be reused for the sub-blocks, and by iteration, we construct a full replica symmetry breaking (FullRSB). But we must not forget that the interest of the matrix q is to take the $\lim_{s\to 0}$ for computing the average free energy. Now, things become 'crazy' [8], but it works. The matrix of $k \times k$, which is now the initial number of replicas and thus the maximal number of replicas breaking the symmetry step, is parameterized by two sets of numbers $m_0, \ldots, m_k$ and $q_0, \ldots, q_k$, with the natural inequality $s \geq m_0 \geq m_1 \ \ldots \ \geq m_k = 1$. But when we make n tend to 0, we perform an analytic continuation of the matrix for $0 \leq s \leq 1$, and this inequality is preserved

$$0 \leq s \leq m_0 \leq m_1 \ \ldots \ \leq m_k = 1, \tag{2.26}$$

And for each subgroup m_i, we associate a q_i such that

$$0 \leq q_0 \leq q_1 \ \ldots \ \leq q_k. \tag{2.27}$$

If we remember, the mean of m_k is the number of diagonal sub-blocks of the matrix q. So, we consider non-integer numbers of subgroups of replicas in the analytic continuation. In the FullRSB framework, i.e. $k \to \infty$, there are an infinite number of subgroups, and $q_i(m_i)$ can be seen as a piecewise function. It tends to be a continuous monotone function $q(x)$ when the discrete set of m_i tends to the interval [0,1].

The replica symmetry breaking (RSB) induces that the replica has an ultrametric (UM) structure. The concept of UM will be defined in Section 4.2 and used in Part III to study the energetic landscape of an array of spinners. The following section will focus on the order parameter of RSB.

2.6 Replica symmetry broken phase

The replica symmetry breaking implies the existence of many different metastable states, labeled $\alpha = 0,1,\ldots$ each with a probability of occurrence ω_α. We can describe the average free energy using a distance matrix Q, where each element represents a distance between two replicas. Edward and Anderson proposed the distance $q_{\alpha\beta}$, as seen in Eq.(2.18). A natural observable is the probability distribution of $q_{\alpha\beta}$ with respect to the weights ω_α of all replicas:

$$P_{\mathcal{J}}(q) = \sum_{\alpha,\beta} \omega_\alpha \omega_\beta \delta(q_{\alpha\beta} - q). \tag{2.28}$$

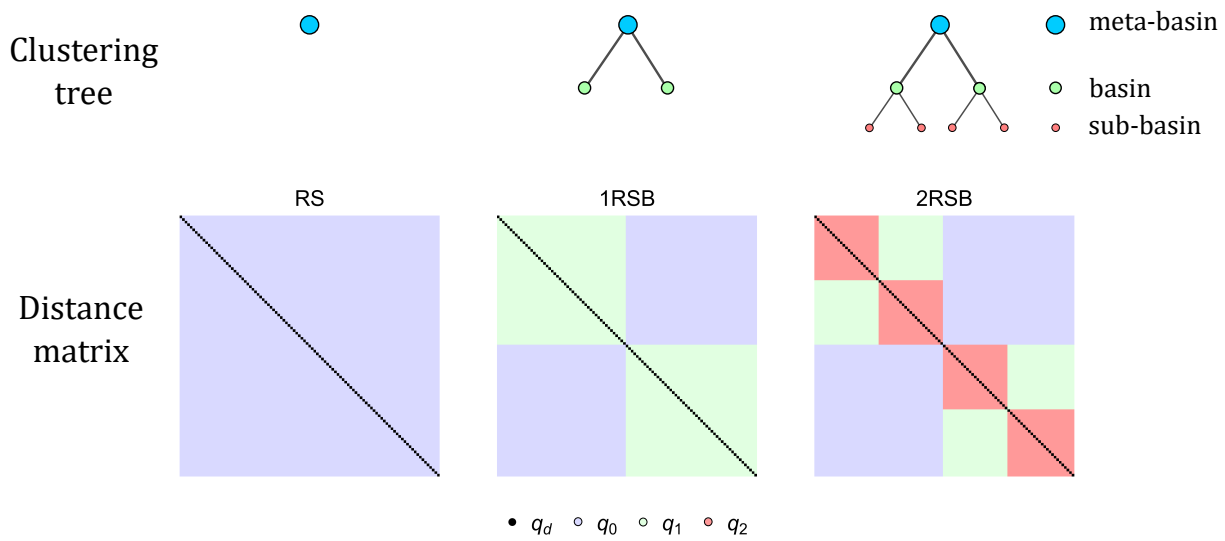

Figure 6: **(All)** Illustration of the replica symmetry breaking process with two points of view: a matrix q where each element q_{ij} represents a distance between replica i and replica j, and a clustering tree that represents clusters of similar replicas. Note that diagonal elements have a given value q_d. **(RS)** In the replica symmetry situation, all replicas are similar, and there is only one value q_0 for non-diagonal matrix elements. All replicas are equidistant, and there is only one cluster. **(1RSB)** In the first step of the replica-breaking process, the main cluster is split into m_1 sub-clusters, here $m_0 = 2$. There are two families of replicas; the distance between replicas of the same family is q_1, and for inter-family replicas, it is still q_0 with $q_1 < q_0$. **(2RSB)** In the second step, each sub-cluster is divided into m_2 sub-sub-clusters, here $m_2 = 2$. Each family is divided into sub-families, introducing a new distance in the matrix, $q_2 < q_1 < q_0$.

If all replicas are symmetric, there is only one value of distance q, and $P_{\mathcal{J}}(q)$ is a delta function. However, if it is a double delta function, we have 1RSB; if there are k delta functions, we have kRSB; and if $P_{\mathcal{J}}(q)$ is continuous, we have FullRSB. We can also consider the average of this observable:

$$P(q) = \overline{P_{\mathcal{J}}(q)}. \tag{2.29}$$

The probability distribution $P(q)$ gives insight into the structure of the solution and the different metastable states present in the system. The properties of $P(q)$, such as the number of peaks, their positions, and their widths, provide information about the nature and complexity of the energy landscape, revealing the intricacies of the spin glass phase.

A glass state, in a replica symmetric phase, samples ergodically a restricted volume of phase space [6]. Indeed, the matrix Q is characterized only by a single number q_0. In 1RSB, the glass is not a simple thermodynamic state anymore, but rather a collection of substates organized into different basins of states. The substates within the same basin are more similar to each other than to substates in two different basins. Generally, for a kRSB, there are k levels of basins: sub-basins, basins, meta-basins, and so on. Each level represents a hierarchy of organization in the phase space of the system [7, 8], see Figure 6. This hierarchy is ultrametric and the concept of replica symmetry broken phase will be used to describe the phase of an array of spinners at zero temperature. But before that, we still need tools to find stable configurations of spinners and that is the topic of the following section.

3 Simulated annealing

The study of many-body systems has always been a challenge, often due to combinatorial analysis resulting in an overwhelming number of possibilities. A notable example is the salesman problem [38], which involves determining the most efficient order to visit a given set of N cities. When dealing with just 10 cities, there are $10! = 3\ 628\ 800$ possible options. Even for small N values, the problem becomes too vast, and it is unrealistic to expect to find the optimal solution. However, it is not the end of the story; we can hope to find a so-called near-optimal solution. This holds for a wide range of problems: Why is the ground state of a spin glass? What are the optimal parameters for machine learning? How can a hundred different electronic components be placed in a minimal area?

In 1953, at Los Alamos, Metropolis proposed the eponymous Metropolis algorithm which is capable of finding configurations of interacting particles that are metastable. It is not the ground state but rather local minima in the energetic landscape [39]. The concept has been a bit generalized by a famous paper of Kirkpatrick [38] as simulated annealing. The annealing process involves heating, for example, a glass, to a high temperature T_{high} and then cooling it to a lower temperature T_{low} at a specified cooling rate α. It is an industrially well-known process that is used to reduce the frustration in a material, thereby improving its solidity and stability [40]. Kirkpatrick has simply translated this concept for general purposes.

The algorithm is given below on the pseudo-code labeled Algorithm 1. Let's consider a spatial configuration of N Ising spins that obey the Edward and Anderson Hamiltonian. This is our initial state. First, we perform a random change of orientation on one spin. This change induces a variation of energy ΔE. If this variation is negative, we accept the change. But if $\Delta E < 0$, the Boltzmann theory says that there is a probability that this non-energetically favorable change will be accepted. This probability is given by

$$P(\Delta E) = \frac{e^{-\Delta E/k_B T}}{Z}, \tag{3.1}$$

where Z is the partition function, k_B is the Boltzmann constant (usually set to 1 for convenience), and T is the temperature. Concretely, when $\Delta E < 0$, we compute a random probability p, and we accept the change if $p < \exp(-\Delta E/k_B T)$.

The strategy of the algorithm involves starting at a high temperature and decreasing it step by step until a lower temperature is reached, reducing the probability of accepting non-energetically favorable changes. For each temperature step, a certain number of Monte Carlo moves are performed. The cooling rate, initial temperature, and the number of changes per step are important parameters. In addition, this algorithm is generalized to many situations by replacing energy with a cost function and temperature with a control parameter [41], making it applicable to a wide range of computational problems. For instance, one might seek to find the quickest car itinerary or determine the spatial distribution of electronic components that minimizes the area [38].

Algorithm 1 Pseudo code for a simulated annealing

Inputs: A system
Initial and final temperatures T_i and T_f
Cooling rate α
Number of iterations per temperature step n
Outputs: A system near that minimization of the cost function
$T = T_i$
repeat
    for n times **do**
        Compute the old energy E_{old}
        Generate a random change in the configuration
        Compute the new energy E_{new}
        if $\Delta E = E_{\text{old}} - E_{\text{new}} < 0$ or $\text{rand}(0,1) < e^{-\frac{\Delta E}{T}}$ **then**
            Accept the new configuration
        else
            Reject the new configuration
        end if
    end for
    Update the temperature: $T \leftarrow \alpha \cdot T$
until $T < T_f$

Simulated annealing will be our major numerical tool to study the energetic landscape in Part III. It is our choice because we can choose the probability to accept unfavorable change and it will be useful to determine is there are a hierarchy in the energetic landscape that characterizes the replica symmetry broken phase as described in Section 2.5 and 2.6. In addition, to characterize this hierarchy we need the concepts of metric and ultrametric distance. This is the subject of the follwing section.

4 Distances

The notion of distance is used to characterize a set of elements in terms of proximity: it helps answer questions like "Is element A closer to element B than to element C?". If we consider a set of cities, we can use the well-known Euclidean distance to characterize their geographical positions: for example, Brussels is at a distance of 102 km from Liège. But the concept of distance is richer than just measuring length. We can define distance as the absolute value of the difference in populations. For example, with this definition, the distance between Liège and the city of Brussels and is 1055 citizens in 2023 [42]. We will discuss what criteria a function must meet to be considered a distance function. Additionally, we will consider the special sets of elements that can be organized into a tree structure, such as a phylogenetic or genealogical tree. The question then becomes: what is the distance between a son and his great-uncle? These concepts are fundamental to studying the energetic landscape of an array of spinners because it is required to determine if we can found a UM structure as in a replica symmetry broken phase that characterize SG.

4.1 Metric distance

4.1.1 Definition

Let's mathematically introduce the concept of metric distance which is in the case of spin glass theory. We must consider a set Ω and an application d, named *distance*, defined by

$$d: \quad \Omega \times \Omega \to A \subset [0,\infty[\quad (\alpha,\beta) \mapsto \mathrm{d}(\alpha,\beta) \tag{4.1}$$

The elements of set Ω can be various things: numbers, the structure of a DNA sequence, species of sharks, and so on. However, the image set of A must be a subset of positive real numbers or zero. The distance between two cities is always positive. In addition, d can be called metric distance and (d,Ω) a metric space if the following properties are verified for all $\alpha, \beta, \gamma \in \Omega$:

$$d(\alpha,\alpha) = 0 \tag{4.2}$$
$$d(\alpha,\beta) \geq 0 \tag{4.3}$$
$$d(\alpha,\beta) = d(\beta,\alpha) \tag{4.4}$$
$$d(\alpha,\beta) \leq d(\alpha,\gamma) + d(\beta,\gamma) \tag{4.5}$$

The first property asserts that the distance between an element of Ω and itself is always zero. The second property imposes that a distance is always non-negative. The third property states that a distance is symmetric: the distance from α to β is equal to the distance from β to α. The last condition is the triangle inequality. It is guaranteed that the distance between Brussels and Liège is either equal to or less than the sum of the distance between Brussels and Antwerp and the distance between Antwerp and Liège. The most famous distance is the so-called Euclidean distance.

4.1.2 Euclidean distance

A well-know example of metric distance, is the euclidean distance on $\mathbb{R}^n$, with $n \in \mathbb{N}$. It is defined as

$$d(\mathbf{x},\mathbf{y}) = \sqrt{\sum_{i=1}^{n}(x_i - y_i)^2}, \tag{4.6}$$

where $\mathbf{x}$,$\mathbf{y} \in \mathbb{R}^n$. For this distance, the triangle inequality (see Eq.4.5) tells us that the shortest distance between tow point is a straight line. There are plenty of other possible examples of distance in $\mathbb{R}^n$, like Manhattan and Chebyshev distance :

$$d_{\mathrm{Manhattan}}(\mathbf{x},\mathbf{y}) = \sum_{i=1}^{n}|x_i - y_i|, \tag{4.7}$$
$$d_{\mathrm{Chebyshev}}(\mathbf{x},\mathbf{y}) = \max_i(x_i - y_i). \tag{4.8}$$

But what kins of distance we can have for a set that is localisation in $\in \mathbb{R}^n$? A answer is provided by Hamming.

4.1.3 Hamming distance

In 1950, Hamming introduced a distance, subsequently named the Hamming (Ha) distance d_{Ha}, to develop algorithms for detecting and correcting errors during the transmission of information [43]. Let's consider a discrete set Ω and two series a and b of Ω of length $n \in \mathbb{N}$.

$$d_{Ha}(a,b) = \sum_{i=1}^{n}(a_i = b_i) \tag{4.9}$$

Where $a_i = b_i$ have a boolean value, i.e 0 or 1. Consequently, the value of this distance corresponds to the number of differences between the two series, element by element. If $\Omega \in \mathbb{R}^n$, then there are a other formulation for Ha distance :

$$d_{Ha}(a,b) = \sum_{i=1}^{n} |a_i - b_i| \tag{4.10}$$

Both of this formulation verify equation 4.1, 4.2, 4.3 and 4.4.

For instance, the dissimilarity between certain DNA strands can be computed using the Ha distance [44]. This aids in comprehending the transcription of DNA and the biological management of errors during DNA duplication. We will use Ha distance to measure the local angular difference between two array of spinner in the Part III.

4.2 Ultrametric distance

4.2.1 Definition

The triangle inequality, as seen in Eq.(4.5), has the marvelous consequence that the considered set can be continuous, such as $\mathbb{R}^3$. However, this property does not hold if we substitute the triangular inequality by a stronger condition, i.e.

$$d(\alpha,\beta) \leq \max(d(\alpha,\gamma),d(\gamma,\beta)), \tag{4.11}$$

where Ω is a discrete set and α, β, and γ are elements of Ω. In this case, we are not discussing metric distance, but rather ultrametric distance and ultrametric UM space [45].For instance, a UM space is a genealogical tree with a genealogical distance: a father and his son have a distance of one, a grandfather and his grandson have a distance of two, etc. Eq.(4.11) imposes that the distance between two brothers is less than or equal to one. A UM space has two remarkable properties. Firstly, it must be a discrete set; indeed, a continuous set cannot satisfy Eq.(4.11) because it implies, unlike a metric space, for a UM space you cannot have 3 points aligned, see Figure 7. Secondly, this discrete set must be isosceles, meaning for α, β, and $\gamma \in \Omega$ we have the corollary:

$$d(\alpha,\beta) = d(\alpha,\gamma) \text{ or } d(\alpha,\beta) = d(\gamma,\beta) \text{ or } d(\alpha,\gamma) = d(\gamma,\beta), \tag{4.12}$$

this implies that there cannot be a brother closer to his father than another. All sets of three points must form an isosceles triangle.

The UM distance and space are suitable for studying the clustering of data, such as phylogenetic trees, genealogical trees, or etymological trees. It is related to the concept of clustering and is used to group data, for instance, to group species into families, orders, or classes.

4.2.2 Ultrametric tree

In graph theory, a graph is a conceptual and mathematical object consisting of E edges and V vertices, designated by $G(E,V)$. It comprises a set of edges connecting another set of vertices. For instance, a highway network can be seen as vertices connecting some cities, represented by the edges. Similarly, this applies to a geometric network.

We will focus on a specific subset of $G(E,V)$, the rooted tree: a graph where any two distinct vertices can be connected by exactly one path. For instance, if the Belgian highway network is represented as a tree, there is only one route from Brussels to Liège. Additionally, the notion of *rooted* means that a vertex can be considered as the parent of all others, akin to the biological concept of the last universal common ancestor (LUCA). In addition, a rooted tree is UM if the value of the edges satisfies Eq.(4.11) [46]. See Figure 7.(c-e).

Furthermore, we typically utilize the concept of a minimum spanning tree [47], which entails constructing a tree over a given set of vertices aimed at minimizing the total length of edges. This concept has proven

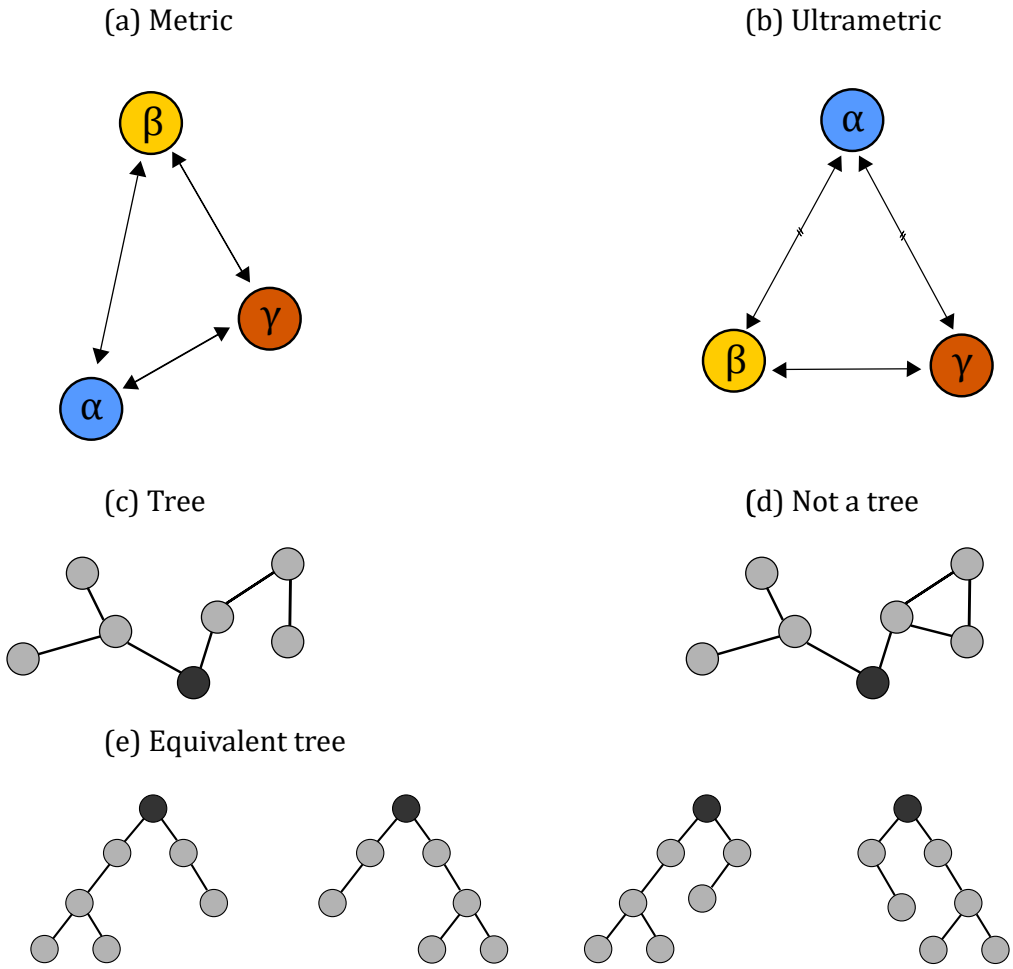

Figure 7: **(a-b)** Let's consider a set Ω and three elements α, β, and γ. This is a schematic representation of all possible distances between these elements. **(a)** In a metric space, we have the triangular inequality which is always verified: it's longer to take a detour. Such a metric space can be continuous. **(b)** An UM space is necessarily discrete and isosceles. Two of the possible distances must be equal, and the third triangle side must be shorter than both equal sides: the distance between sisters can be shorter than the distance between each sister and their mother, but not longer. **(c)** Illustration of a tree graph, where each pair of vertices is connected by exactly one path. Additionally, the dark gray element represents the root of the tree, the parent of all others. **(d)** Conversely to **c**, it is not a tree because three edges form a triangle, so the vertices of this triangle are connected by two possible paths. **(e)** For a same rooted Universal Minimum (UM) tree, there are many possible representations; there is an exponential increase in the number of trees with elements.

to be highly useful in numerous practical problems, such as connecting all European capitals via highways while adhering to the constraint of minimizing the total highway length.

The concept of UM and a tree is connected to RSB theory, see Section 2.5 and 2.6, and they will be used to determine how far from UM are some metric distance, described in Section 6, applied on a set of spinners configurations. Some indicators to quantify a difference between metric and ultrametric distances will be discussed in Section 4.4.

4.3 Distance matrices

Another approach to categorizing a set of data is through the utilization of a distance matrix. This involves employing a function d, often referred to as similarity, which can be a metric or a UM distance, along with a designated set Ω. In concrete terms, we simply need to define the matrix $M_{\alpha\beta} = d(\alpha,\beta)$, where each element is the distance between elements α and $\beta \in \Omega$. Is there a quick way to visualize all clusters in Ω concerning d.

Furthermore, simply computing the matrix distance is insufficient. We must also sort the rows and columns to highlight clusters within the data. To achieve this, we require a definition of similarity between rows and columns. Placing them side by side is essentially comparing them using another distance metric. In this instance, the Euclidean distance may be suitable.

For instance, if we consider the set of real numbers:

$$A = \{-0.961, -1.49, -1.489, -1.955, -1.709, -2.219, -2.524, -2.551, -2.553, -2.58, -2.608\}$$

and the distance $d(\alpha,\beta) = |\alpha - \beta|$ with α and $\beta \in A$, we can construct the matrix on Figure 8: each element corresponds at a distance between a pair of element. A is a set of the energy on the stable configuration of a 2 by 2 array of spinners that will be studied in Part III Section 5.

4.4 Comparison of metric and ultrametric distances.

We will discuss how we can quantify how metric distance is from ultrametricity. It will be useful to determine is the energetic landscape of an array of spinners is ultrametric or not with some given distance.

4.4.1 Subdominant ultrametric distance

Let's consider a metric space (d, Ω), where d represents the metric distance on the set Ω. We can pose the question: what is the UM distance, denoted as d', that best approximates d? The first step in answering this question is to define what we mean by "closest". Typically, this means minimizing the expression:

$$\sum_{\alpha,\beta\in\Omega} |d(\alpha,\beta) - d'(\alpha,\beta)|. \tag{4.13}$$

Because a distance is, by definition, greater than or equal to zero, it is interesting to study UM distances that are less than or equal to the metric distance. Concretely, we define the set $U^<$ of d' that is smaller or equal to d. We use the notation $d' \leq d$, which means that $d'(\alpha,\beta) \leq d(\alpha,\beta)$ for all α and $\beta \in U$. The set $U^<$ is then given by:

$$U^< = \{d' \in U \mid d' \leq d\}. \tag{4.14}$$

In other words, $U^<$ consists of all possible ultrametric distances d' on the set U that is less than or equal to the original metric d. So, we can denote the subdominant ultrametric distance (SUM) $d^<$ as:

$$d^< = \max_{d'\in U^<} d'. \tag{4.15}$$

It is the best approximation of metric distance by an UM distance.

0.	0.529	0.528	0.748	0.994	1.258	1.563	1.59	1.592	1.619	1.647
0.529	0.	0.001	0.219	0.465	0.729	1.034	1.061	1.063	1.09	1.118
0.528	0.001	0.	0.22	0.466	0.73	1.035	1.062	1.064	1.091	1.119
0.748	0.219	0.22	0.	0.246	0.51	0.815	0.842	0.844	0.871	0.899
0.994	0.465	0.466	0.246	0.	0.264	0.569	0.596	0.598	0.625	0.653
1.258	0.729	0.73	0.51	0.264	0.	0.305	0.332	0.334	0.361	0.389
1.563	1.034	1.035	0.815	0.569	0.305	0.	0.027	0.029	0.056	0.084
1.59	1.061	1.062	0.842	0.596	0.332	0.027	0.	0.002	0.029	0.057
1.592	1.063	1.064	0.844	0.598	0.334	0.029	0.002	0.	0.027	0.055
1.619	1.09	1.091	0.871	0.625	0.361	0.056	0.029	0.027	0.	0.028
1.647	1.118	1.119	0.899	0.653	0.389	0.084	0.057	0.055	0.028	0.

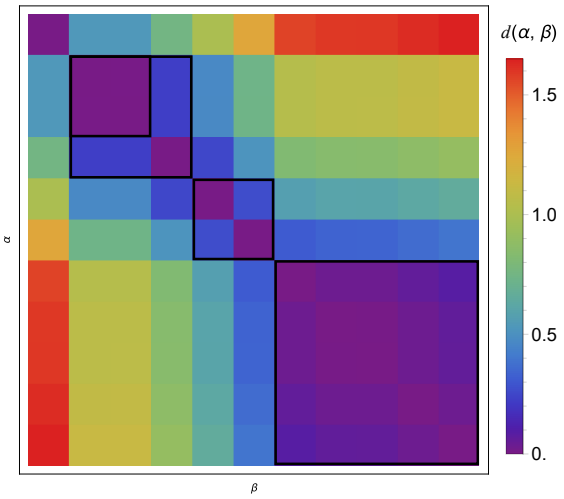

Figure 8: **(All)** We have computed the distance matrix of set A using the distance metric $d(\alpha,\beta) = |\alpha - \beta|$, where α and β are elements of A.Additionally, the matrix can be sorted with respect to the Euclidean distance $d_{ab} = \sqrt{\sum_i (a_i - b_i)^2}$, where a and b represent rows of the matrix.**(Left)** Numerical representation of the distance matrix. **(Right)** A color representation of the distance matrix: each element is associated with a colored pixel. The black squares are used to highlight clusters of elements of sizes 2, 3, and 5.

4.4.2 Ultrametricity indicators

In practical terms, computing the SUM or any other UM approximation of a metric distance requires a method for measuring the discrepancy between a metric distance and another UM. We need an indicator that shows how far we deviate from ultrametricity. One potential approach is as follows [48]:

$$\Delta_k(d',d) = \left[\sum_{\alpha,\beta \in U} |d(\alpha,\beta) - d'(\alpha,\beta)|^k \right]^{1/k}, \quad k > 0 \tag{4.16}$$

Clearly, the maximum value of $\Delta_k(d',d)$ is reached when $d' = d^<$. Furthermore, when dealing with different sets U of varying cardinality N, it is useful to normalize by N [49]. For the case where $k = 2$, the expression is given by:

$$D^x = \sqrt{\frac{1}{2N} \sum_{\alpha,\beta \in U} (d^x(\alpha,\beta) - d'(\alpha,\beta))^2} \tag{4.17}$$

Another concept for quantifying the distance between metric and ultrametric distances is the degree of ultrametricity [48]. It is defined as follows:

$$\mathfrak{D} = \frac{\sum_{\alpha,\beta \in U} d(\alpha,\beta) - d^<(\alpha,\beta)}{\sum_{\alpha,\beta \in U} d(\alpha,\beta)} \geq 0 \tag{4.18}$$

Certainly, we have $0 \leq \mathfrak{D} \leq 1$. It is an intrinsic property of a discrete set. The strength of this indicator lies in its normalization by the metric distance. It can be used to compare different metric distances.

Now we have the theoretical background to study the degree of ultrametricity of the configurational space of an array of spinners, but need only one thing more: a numerical way to compute the ultrametric distance on a given set. This is the topic of the following section.

5 Clustering

5.1 Concepts

Clustering is a widely used tool and concept in science. It can be used to reduce data volume, construct phylogenetic or genealogical trees, or group distinct geographic areas in urban settings, among other applications. The idea is to group similar data points into the same cluster, and then further group similar clusters into sub-clusters. This process allows us to construct a tree graph of all data based on a similarity function [46, 50].

Clustering can be represented in various ways, such as through a distance matrix, illustrated in Figure 8, or a tree graph. It's also known as hierarchical ordering since data are organized according to their proximity. Clustering serves as a method to measure how far a metric distance deviates from ultrametricity within a given set.

5.2 Algorithm

5.2.1 General pseudo code

Clustering is typically performed using numerical methods and constitutes a significant area of research in computational science [46, 51, 52]. The concept is straightforward and is illustrated in pseudo-code labeled Algorithm 2.

Consider a set of N elements and a similarity function between two elements. Initially, each element is placed in its cluster. Then, iteratively, clusters are merged based on their proximity according to the similarity function. This process continues until only one cluster containing all elements remains. Additionally, during the merging process, information about the ultrametric distance between all elements is stored.

Algorithm 2 Pseudo code of a simple clustering algorithm [51]

```
1: Inputs: A distance matrix N × N
2: Outputs: An ultrametric distance matrix between 2 states
3: Initialization: Place each state in a single-element cluster C_1, C_2, ..., C_N.
4: repeat
5:     for each cluster C_i do
6:         if C_i has not been merged with another cluster then
7:             Merge C_i with the nearest cluster
8:             Mark that C_i has been merged
9:         end if
10:    end for
11: until Only one cluster remains
```

5.2.2 Similarity between cluster

The first step is straightforward: merging single-element clusters. However, the complexity arises when we encounter the question: what is the similarity between clusters containing more than one element? This is not obvious, as we are now dealing with a set of sets. Numerous options have been studied in the literature

[46, 51, 52], and three simple answers have been formulated:

$$\text{Single link:} \quad d(A,B) = \min_{a\in A, b\in B} d(a,b), \tag{5.1}$$

$$\text{Complete link:} \quad d(A,B) = \max_{a\in A, b\in B} d(a,b), \tag{5.2}$$

$$\text{Average link:} \quad d(A,B) = \frac{1}{n_A n_B} \sum_{a\in A, b\in B} d(a,b). \tag{5.3}$$

where A and B are two sets. In the single link method, the distance between two sets is the minimum distance among all pairwise distances between one element from each set. For the complete link method, it is the maximum distance. The average link method considers the average of all pairwise distances between elements of the two sets.

5.3 Optimal ordering and sorting

A related problem to clustering is the sorting of data, which serves different purposes. While clustering is driven by scientific objectives, sorting is often done for pedagogical reasons. Clustering aims to provide insights and patterns within data, whereas sorting is essential for presenting this information in an organized manner. Various methods exist for sorting data, each tailored to different needs. For instance, when dealing with a tree structure with $n-1$ internal nodes, there can be 2^{n-1} distinct tree representations (see Figure 7.(e)) [52].

However, there's no one-size-fits-all solution for sorting, as it depends on the specific context and requirements. The ultimate goal is to present the data clearly and comprehensively. For example, when dealing with a distance matrix, arranging rows and columns adjacently can be helpful for visualization and analysis.

Finally, we can implement a clustering algorithm and apply it on a set of spinner configurations, to construct an ultrametric distance. We have all we need to start the exploration of configurational space and the energetic landscape of any arrays of spinners.

Part III

Personal contribution

1 Introduction

The objective of this thesis is to investigate whether an array of spinners can emulate an experimental and macroscopic spin glass at zero temperature. Essentially, it aims to verify if the energy landscape exhibits a vast number of local minima and whether these minima form an ultrametric tree.

To accomplish this, we will begin by constructing a theoretical framework based on experimental observations. Subsequently, we will examine the scaling of the stable configuration count in the function of the number of spinners. Finally, we will explore the configuration space through simulated annealing and compute a measure of the ultrametricity of the set of stable configurations.

Furthermore, we will investigate the influence of the number of spinners N, the lattice parameter L, and an external magnetic field B.

2 Experimental setup

2.1 Characteristics of a Spinner

In this study, we will consider the so-called "spinner", essentially composed of multiple magnetic dipoles, which allows each dipole to rotate around a fixed point while maintaining a consistent orientation relative to one another. Our attention is directed towards a specific configuration of the spinner, which we have fabricated using 3D printing and approximate macroscopic point dipoles. Images illustrating the spinner are displayed in Figure 9 (a-c). It is a spinner with three dipoles arranged radially and separated by 120 degrees. We only consider spinners with three dipoles, each with the same absolute value. Two dipoles are pointing outside (coloured in red), while the third one is pointing to the center inner (coloured in blue) as seen in Figure 9 (d). In addition, we place these spinners on a triangular lattice with L as the lattice parameter. In conclusion, our system is characterized by four parameters

- the lattice parameter L
- the length l of branches
- the magnetic moment μ of the dipoles
- the radius R central part of the spinner.

They are all illustrated in Figure 9 (e). Note that l and R are fixed to 5 and 3 mm on the experimental setup, respectively. Moreover, it's worth noting that we will not consider energy dissipation due to friction when a spinner spins. Our focus lies not in the dynamics of a spinner lattice but rather in the metastable configurations where the spinners are in static equilibrium. The spinners will be placed on a lattice where they can interact.

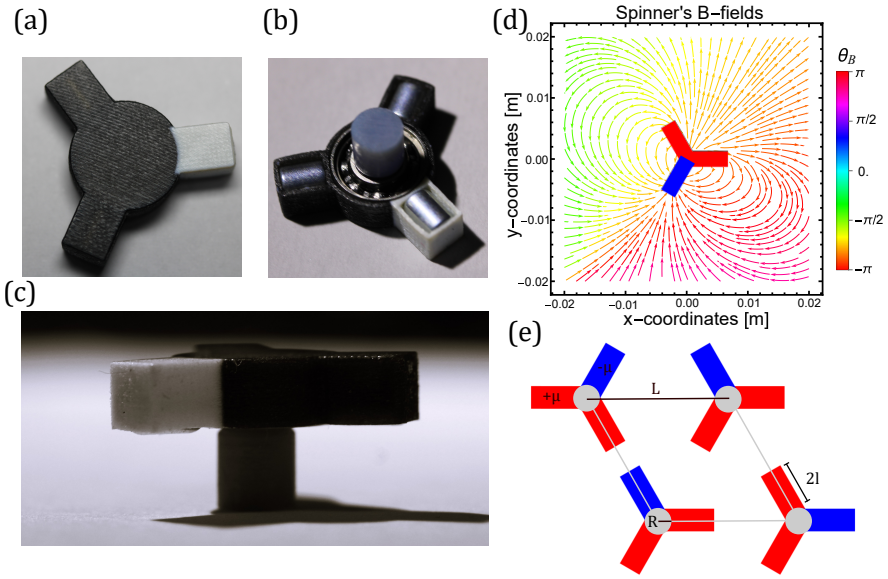

Figure 9: **(a)** Top view of the spinner with a color code: white for the inner magnetic moment, black for the outer magnetic moment. **(b)** Downward view highlighting the ball bearing facilitating rotation with minimized friction. **(c)** Side view offering a comprehensive look at the experimental setup. **(d)** Schematic representation of a spinner in the experimental case, showing magnetic fields generated. Correspondence between white and blue, and black and red. **(e)** Illustration of key parameters of a spinner lattice: lattice parameter L, magnetic moment μ, radius R, and arm length $2l$. Note: magnetic moment is approximated as a dipole at the arms' center.

2.2 Lattice of spinners

The spinners can be arranged on a lattice. Specifically, we can place the axis enhancer within the ball bearing, in a hole of diameter sufficiently similar so that it cannot rotate. One can rotate a spinner and see the effect of perturbation. Furthermore, a magnetic field can be apply. We will focus on triangular lattice without empty site, an axample can be see on Figure 10.

2.3 Convention

We must establish practical conventions for reference angles. We will consider a triangular lattice where each spinner has six neighbours, except for border spinners. We designate the state $S_i = 0$ as a spinner with a red arm aligned along the x-axis to the right and the blue arm below the x-axis. Additionally, we consider angles in a counter-clockwise convention. All of this convention are depicted in Figure 10.

Additionally, we will establish a convention for the renormalization of energy. We will consider that an energy of 1 corresponds to the absolute value of the interaction energy of two aligned point dipoles at a distance of $L - 2l - 2R$.

We have now describe our experimental setup and we have to pose a theoretical spin glass poit-of-view for us spinners. It will be done is the next section.

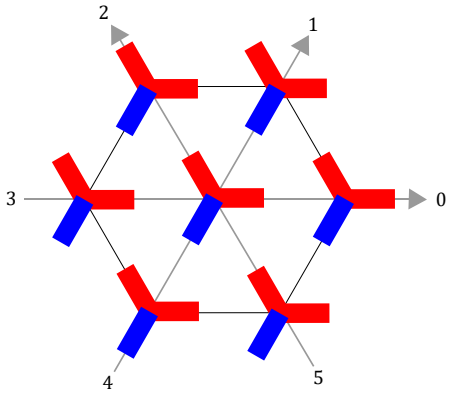

Figure 10: The spinners are arranged on a triangular lattice, with each spinner having six neighbors. Consider a spinner and all its neighbors in the state $S_i = 0$. Obviously, we know that the interaction is not isotropic. Indeed, the interaction depends not only on the states of both spinners but also on the relative orientation of the spinners. This relative position is labeled from 0 to 5 on the diagram.

Figure 11: Example of local distortion from the six-angle hypothesis. The strength of the repulsion of an alignment of two outer magnetic moments creates a local misalignment. This is analogous to a well-known Jahn-Teller distortion in condensed matter physics [54].

3 Spin glass framework

The initial step involves developing a suitable theoretical framework to align with SG theory and the experimental setup of the spinners. The main idea is that a spinner can be seen as a p-state spin glass [53], where each spin can occupy one of p distinct states. For example, an Ising spin is a 2-state spin. We will start from experimental observations in Section 3.1 to propose a discreet model of an array of spinners. After, we will naturally propose a Hamiltonian for this discreet model.

3.1 Experimental observation

When we manipulate the experimental setup manually or with a magnetic field, we observe that the hypothesis of discretization into six angles is a good approximation. This hypothesis is largely verified. However, it should be noted that deviations from this hypothesis may be observed, with the main deviation illustrated in Figure 11: two black arms that are not perfectly aligned. This is due to the strong local repulsion between anti-aligned magnetic dipoles. This is analogous to a well-known Jahn-Teller distortion in condensed matter physics [54]. However, this is not a problem because we can treat this misalignment state as a deviation from a unique state without misalignment. Therefore, it is not problematic for the study of energetic landscape and configurational space.

3.2 Discrete model

We will consider spinners as 6-state first-neighbor spin glass. Specifically, we will discretize the angle of a spinner into only 6 integer angles, multiples of $\pi/3$ radians. For simplicity, we will label these angles as $0, \ldots, 5$. So, a spinner i can be represented by $S_i \in \Omega_i = \{0, \ldots, 5\}$, and a configuration $\underline{S}$ of N spinners is a point in the configurational space $\Omega = \bigotimes_{i=1}^{N} \Omega_i$. Furthermore, the set of spinner states, with the modulo addition, forms a group [55]. As depicted in Figure 12, the discretization will have an impact on the size of the configurational space and the number of metastable states.

In this framework, the interaction between two spinners is always represented by the sum of nine dipole-dipole interactions, each corresponding to a specific relative position between the two spinners. However, this interaction can only take 36 distinct values because there are only 6 possible angles for both spinners due to the choice of discretization. This specific interaction will be discussed in the next section.

3.3 Interactions between 2 spinners

The first question about two spinners is: How do two spinners interact? Since a spinner is composed of 3-point dipoles, a two-spinner interaction is simply the addition of 3×3 dipole-dipole interactions. This interaction between two dipoles k and m is given by the following potential:

$$U_{dd}(\mu_k, \mu_m) = \frac{\mu_0}{4\pi} \left(\frac{\vec{\mu}_k \cdot \vec{\mu}_m}{r^3} - \frac{3(\vec{\mu}_k \cdot \vec{r})(\vec{\mu}_m \cdot \vec{r})}{r^5} \right). \tag{3.1}$$

We will assume that all dipoles are identical in strength, i.e., $\mu_k \equiv \mu$. Additionally, we have a vector $\vec{r}$ joining the positions of both magnetic moments μ_k and μ_m. In the particular case where spinners are aligned along the x-axis and dipoles can only take six discrete azimuthal angles as multiples of $\pi/3$, we have:

$$\vec{r} = (L + (R+l)(\cos S_k\pi/3 - \cos S_m\pi/3))\vec{e_x} + (R+l)(\sin S_k\pi/3 - \sin S_m\pi/3)\vec{e_y}, \tag{3.2}$$

and

$$U_{dd}(S_k, S_m) = \frac{\mu_0\mu^2}{4\pi} \left(\frac{\cos(\pi/3(S_k - S_m))}{r^3} - \frac{3(\vec{e}_{\mu_k} \cdot \vec{r})(\vec{e}_{\mu_m} \cdot \vec{r})}{r^5} \right). \tag{3.3}$$

We observe that U_{dd} is dependent on both dipole states and their orientations, denoted by S_k and S_m. A dipole state is defined analogously to a spinner state but with indices k and m replacing i and j. So, we can now compute the spinner-spinner interaction as

$$U_{ss}(S_i,S_j) = \sum_{k,m=1}^{3} U_{dd}(S_k,S_m). \tag{3.4}$$

It may exhibit complex behaviour with numerous metastable states, as illustrated in Figure 12(a-b). Consequently, a lattice of N spinners, whose energy is the sum of all spinner-spinner interactions, can display complex behaviour and possess a highly diverse energetic landscape.

As explained in section 2.3, we define $E_{\text{ref}}(L)$ to correspond to the absolute value of the energy of two dipoles with aligned spinner arms between spinners, as depicted at the center of Figure 12(b). We then normalize energy by $E_{\text{ref}}(L)$ to obtain dimensionless observables, ensuring that an energy of 1 corresponds to the energy of two aligned dipoles. These are the main characteristic energy values of our system. Figure 12(a) shows us that some metastable states in the discrete model are surrounded by high energetic barriers, i.e. $\Delta E \sim 1$, or smaller barriers. In addition, we can find in Figure 12(c) all metastable configurations. Finally, we can now define a Hamiltonian based on $U_{ss}(S_i,S_j)$.

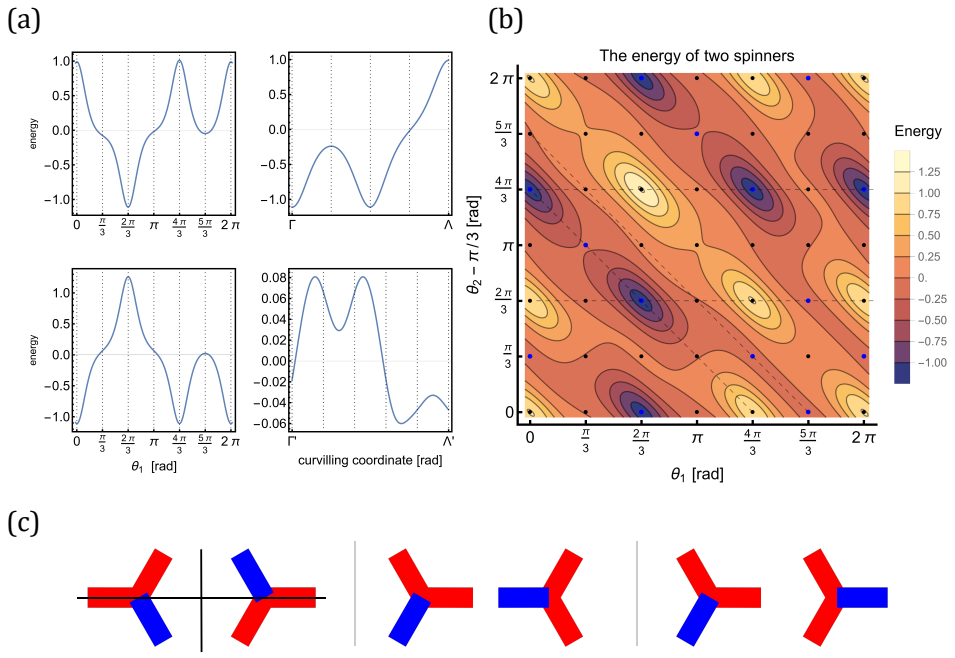

Figure 12: (**a**) We have $\Gamma = (0,\ 4\pi/3)$ and $\Lambda = (5\pi/3,\ 0)$, and $\Gamma' = (0,\ 4\pi/3)$ and $\Lambda' = (5\pi/3,\ 0)$. The plot displays a cross-section of the energetic landscape. We can observe deep minima as well as others that are slightly less profound. (**b**) Contour plot of the energy as a function of both angles of the two spinners. We have plotted $\theta_2 - \pi/3$ to highlight the axial symmetry of the energy landscape. Additionally, the bullets represent the points considered in the discrete configuration space; the black ones are not metastable, but the blue ones are metastable. In addition, dotted strips are the cut shown in **a**. (**c**) Here are the three elementary metastable states. All 10 metastable states can be constructed from these three, with the two mirror planes shown as black lines. (**All**) We consider a 2×1 lattice for $L = 25$ mm.

3.4 Hamiltonian

We have established a model for the object called the spinner and derived the spinner-spinner nearest neighbour interaction. The next step is to introduce a Hamiltonian that governs the behaviour of a lattice of $N \times N$ spinners. In general, the Hamiltonian of a lattice of spinners can be expressed as

$$H_N(\underline{S}) = \frac{1}{2}\sum_{ij}^{N} J_{S_i S_j ij}, \tag{3.5}$$

where $J_{S_i S_j ij}$ is an $6 \times 6 \times N \times N$ tensor. This tensor depends on the positions i and j of the spins and their respective states S_i and S_j. Experimentally, it is justified to consider only nearest-neighbour interactions, denoted by $\langle ij \rangle$, so H_N takes the form:

$$H_N(\underline{S}) = \frac{1}{2}\sum_{\langle ij \rangle}^{N} J_{S_i S_j k_{ij}}. \tag{3.6}$$

Because this is a nearest-neighbour interaction, we can use a tensor $J_{S_i S_j k_{ij}}$ of $6\times6\times6$ parameter, representing the interaction between two first neighbour spinners. The third dimension k_{ij} is because there are six possible nearest neighbours, and this interaction is anisotropic, as shown in Figure 10. Here, $k_{ij} \in \{0, \ldots, 5\}$ denotes

the relative position of spinner j with respect to spinner i. Indeed, the lattice cell has an axis C_6 of symmetry, but a spin has only a C_1 symmetry. Despite the C_6 axis ensuring that only 36 elements of $J_{S_iS_jk_{ij}}$ are different, within these 36 elements, only 13 distinct values exist. The energy of interaction between two spinners is symmetric under the action of the double mirror plane described in Figure 12(c). Therefore, the elements of the matrix $J_{S_iS_j0}$ have a degeneracy of four, two, or one. For $L = 25$ mm, concerning the energy convention described in section 2.3, we have

$$\begin{aligned}
J_{000} = J_{110} = J_{330} = J_{440} &= -0.017979 \\
J_{020} = J_{510} = J_{530} = J_{420} &= -0.046878 \\
J_{040} = J_{130} = J_{400} = J_{310} &= -0.075333 \\
J_{050} = J_{210} = J_{230} = J_{450} &= -1.109605 \\
J_{120} = J_{500} = J_{540} = J_{320} &= -0.019704 \\
J_{150} = J_{200} = J_{240} = J_{350} &= +0.066052 \\
J_{010} = J_{430} &= +1.011013 \\
J_{030} = J_{410} &= +0.988990 \\
J_{100} = J_{340} &= +0.259880 \\
J_{140} = J_{300} &= -0.238726 \\
J_{220} = J_{550} &= +0.022133 \\
J_{250} &= +1.258910 \\
J_{520} &= +0.150482
\end{aligned}$$

The matrix is not symmetric because the interaction is not symmetric, i.e., $J_{S_iS_j0} \neq J_{S_jS_i0}$ if $S_i \neq S_j$.Note that the minimum ΔE is $\Delta E = |J_{000} - J_{120}| = 0.001725$ and the maximum is $\Delta E = |J_{250} - J_{140}| = 1.497636$. It's important to know the energy difference range to proceed with simulated annealing, which directly involves the ratio $\Delta E/T$. We set $k_B = 1$ as it is commonly done in computational and theoretical developments on spin glass [7]. We have now a complete theoretical framework to describe our experimental setup, we need yet define what is a metastable state to study the energetic landscape numerically.

4 Lattice and metastability

As explained in Part II, the glassy phase is characterized by an energy landscape with an infinity of local minima, in the thermodynamic limit, that correspond to many metastable configurations. To study our system, we need a definition of a metastable configuration.

4.1 Metastability criteria

We will say that a configuration $\underline{S}$, of N spinners, is metastable if, for all $i \in N$, a change of ± 1 of S_i leads to an increase in energy. Note that if one change leads to another configuration $\underline{S}'$ with the same energy, we consider both $\underline{S}$ and $\underline{S}'$ as metastable. For numerical considerations, due to the finite precision of floating numbers in C language, we use the following practical criterion for metastability

$$E < E_{\text{change}} + 10^{-14}, \tag{4.1}$$

where E is the energy of $\underline{S}$ and E_{change} is the energy of $\underline{S}$ after a change of one spinner by ± 1. We choose 10^{-14} because we are working with double precision, which offers 16 significant decimal digits [56], and we include a safety margin of 10^{-2}. We can do this because the minimal ΔE is 0.001725 (see section 3.4), and we will always ensure to work within the same energy range. With this definition we can make a first study on the number of metastable state over the cardinality of the configurational space.

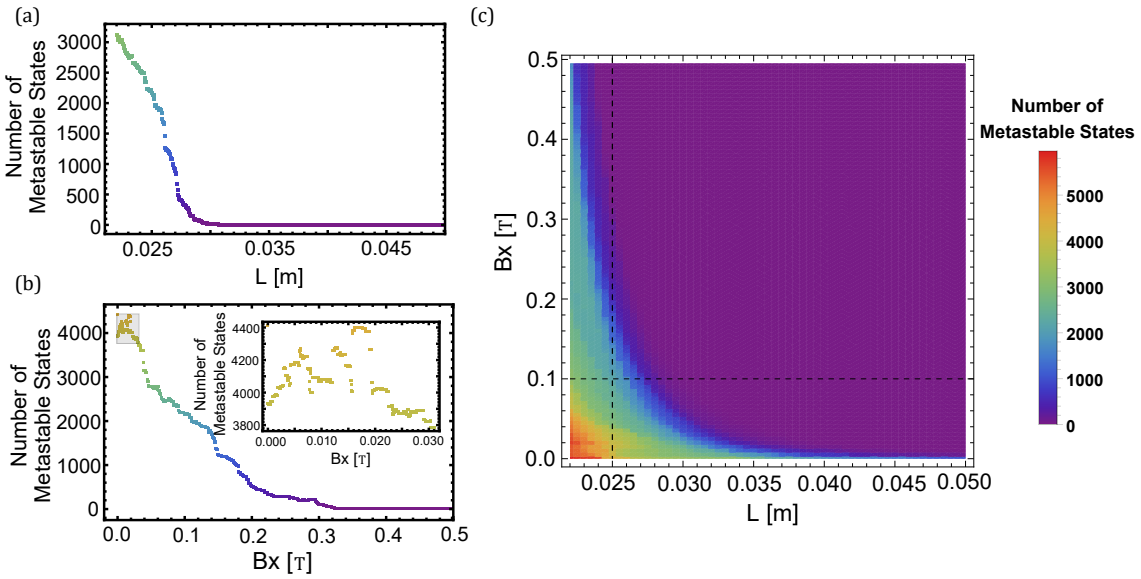

Figure 13: **(All)** Number of metastable states N_{meta} for a 3x3 lattice plotted against B_x and L. **(a)** Variation of N_{meta} with L at $B_x = 0.1$ T. The count decreases until only one state remains, indicating fewer available energetic minima as spinners are more densely packed. **(b)** Dependence on B_x for $L = 0.25$ mm. N_{state} decreases until only one state persists. A zoom-in reveals an unexpected observation: a weak magnetic field can increase the number of metastable states, although it seems counterintuitive that dominant spinner interaction and the energetic landscape become smoother. **(c)** N_{meta} for a range of L and B_x. If B_x is strong enough, only one metastable state remains.

4.2 Number of metastable states

We know that the cardinality of the configurational space of a system of N spinners scales as 6^N. For example, if we consider $N = 32$, the number of states $6^{32} \sim 10^{24}$ is of the same order as the estimated number of stars in the observable universe [57]. However, we do not yet know how many states are metastable, and this is an important question.

$N = N_x \times N_y$	6^N	N_{meta}	$6^{0.522N}$
1×2	36	10	/
2×2	1 296	38	42
3×3	10 077 696	4415	4528
4×4	2 821 109 907 456	3 157 857	3 157 856

Table 1: We consider a lattice with $L = 0.25$ and without external B-fields. Note that all states for 2x1 are displayed in Figure 12(c), and for 2×2 in Figure 14(c-d).

We will concentrate on a select few cases that can be exactly resolved through brute force, i.e. by testing every configuration. In Table 1, you can observe the number of states and metastable states N_{meta} for lattices of two, four, nine, and sixteen spinners. We notice a significant increase in the difference between the counts of states and metastable states, suggesting that there are very few metastable states relative to the cardinality of the configurational space, differing by many orders of magnitude. When we perform a fitting of the parameter a in $6^{a \times N}$ to estimate N_{meta}, we find

$$N_{meta} = 6^{0.522N}. \tag{4.2}$$

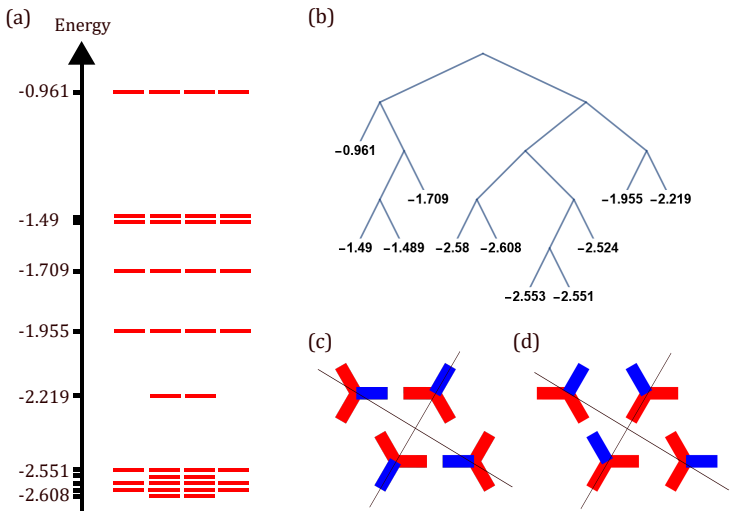

Figure 14: **(All)** We consider a 2 by 2 lattice of spinners with $L = 25$ mm. **(a)** Schematic representation of the 38 metastable states. The double or quadruple degeneracy is explained by the two mirror planes of the 2 by 2 lattice. **(b)** Clustering tree based on the energy values of metastable states. It can also be viewed as a distance matrix in Figure 8. (b). **(c)** State with a double degeneracy, where both mirror planes have the same effect. **(d)** State with quadruple degeneracy.

In addition, we have studied the behaviour of N_{meta} when applying a magnetic field B_x in the x-direction and varying the lattice parameter L, as shown in Figure 13. We observe that an increase in L or B_x leads to a rapid decrease in N_{meta}. This decrease is not linear but exhibits a jump or local minima. It can be the first indication of a hierarchical structure of the energetic landscape. Moreover, a small B_x can actually increase N_{meta}.

5 Example

After defining our system, its Hamiltonian, and estimating the number of metastable states, we conducted a pedagogical study focusing on a two-by-two lattice. This study aimed to determine the total number of states and metastable states, their respective energies, and their distribution in the configurational space.

A system of four spinners, with $L = 25$ mm, has 1296 different states, but only 42 are metastable. We can compute the total energy for these metastable states and plot them on an energy diagram, as shown in Figure 14(a). We observe that for the same energy, we have two or four different states, indicating a degeneracy. The quadruple degeneration of an energy level arises from the presence of twin-plane mirrors characteristic of the diamond cell. Sometimes, the degeneration is only double due to the identical effects of the twin plane mirrors, see Figure 14(c-d).

To study the distribution of metastable states in the configurational space, we will use clustering algorithms with the distance metric given by

$$d(\alpha,\beta) = |E_\alpha - E_\beta|. \tag{5.1}$$

We will only consider the eleven different energy levels. The result will show that we can isolate clusters of sizes five, three, and two. These clusters consist of configurations with very similar energies. Using clustering, we can construct a tree as shown in Figure 14(b) and a distance matrix as illustrated with an equivalent example to Figure 8.

Finally, we have shown that energy levels can be grouped into clusters of similar energy. In Section 6, we observed that there are a huge number of different distances, which are choices that we have to make. For instance, some distances may be related to energy differences, while others may be related to configurational differences such as Hamming distance.

6 Distances considered

We will now define the distance metric that we will use, focusing on two characteristics of lattice spinners: the density of energy and the states of spinners. As found in the literature, we will work with the Hamming distance and energy difference [49].

Let's define the number of neighbour n_i of i^{th} spinner and the function diff :

$$\text{diff}(x) = \min(x^2,(6-|x|)^2) \tag{6.1}$$

It ensures that the difference between two angles is less than or equal to 3 at most, which makes it possible to calculate the minimum Hamming distance between 2 spinners. We define four different distance between replica α and $\beta \in \Omega$:

- General energy (GE) distance
$$d^N_{GE}(\alpha,\beta) = \frac{|E^\alpha - E^\beta|}{N} \tag{6.2}$$
It can be seen as the global energy difference per spinner.

- Local energy (LE) distance
$$d^N_{LE}(\alpha,\beta) = \sqrt{\frac{1}{N}\sum_{i=1}^{N}(E^\alpha_i - E^\beta_i)^2} \tag{6.3}$$
Here, we sum the local energy differences, which are the interaction energies of one spinner with its nearest neighbours.

- Hamming (Ha) distance
$$d^N_{Ha}(\alpha,\beta) = \sqrt{\frac{1}{N}\sum_{i=1}^{N}\text{diff}(S^\alpha_i - S^\beta_i)} \tag{6.4}$$
We sum the differences in the orientations of spinners, akin to the classical Hamming distance, as shown in Eq. (4.10).

- Invariant Hamming (IHa) distance
$$d^N_{IHa}(\alpha,\beta) = \sqrt{\frac{1}{N}\sum_{i=1}^{N}\sum_{j=1}^{n_i}\text{diff}(S^\alpha_i - S^\alpha_j - S^\beta_i + S^\beta_j)} \tag{6.5}$$
The difference with the Ha distance is that we sum the differences in the state between a spinner and its nearest neighbours to be locally invariant under C_6, C_3, and C_2 rotation.

Each distance is normalized by the number of spinners to allow for comparison between lattices of different sizes. Additionally, we note that the concept of distance is related to the notion of a dissimilarity

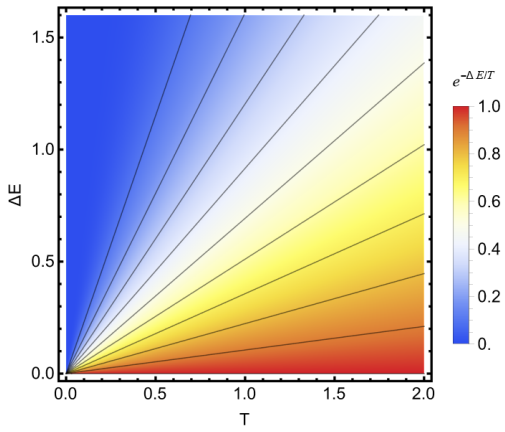

Figure 15: Density plot of the Boltzmann factor $\exp(-\Delta E/T)$, where we have set $k_b = 1$. The black solid line corresponds to probabilities from 0.1 to 0.9 in steps of 0.1. The energy range corresponds to the maximal range that we can have in our system and with the energy nondimensionalization convention for $L = 25$ mm.

function such as $q_{\alpha\beta}$, as defined in Eq.(2.18), with a relation referenced in [58],

$$d_{\alpha\beta} = 1 - \frac{q_{\alpha\beta}}{\max_{\alpha,\beta}(q_{\alpha\beta})}. \tag{6.6}$$

We have now a set of distances to test if the configurational space of an array of spinners is ultrametric or not. We will be simulation after a quick description of the methods used for simulation.

7 Methods for simulations

We will employ computational methods to investigate the configurational space of a lattice composed of spinners. For simulation purposes, we have access to six supercomputers at the high-performance computing center CÉCI (Consortium des Équipements de Calcul Intensif). The code developed for this master's thesis is written in C, and we have utilized OpenMP for extensive parallelization.

Implementing a spinner lattice and a function to compute interaction energy is straightforward. Additionally, we will utilize a simulated annealing algorithm [38, 39], discussed in section 3, to explore the energetic landscape. It's crucial to ensure that this code remains thread-safe during parallelization. This algorithm requires four parameters:

- the initial annealing temperature T_0 .
- the final annealing temperature T_f .
- $0 \leq \lambda < 1$ representing the annealing cooling rate. To decrease the temperature, we multiply T_0 by λ until it reaches T_f.
- n_{step} defines the number of random changes for a temperature step: $n_{\text{step}} \times N_x \times N_y$.

We have shown the behaviour of $\exp(-\Delta E/T)$ is depicted in Figure 15. The probability of accepting an unfavourable energetic change decreases quickly when ΔE increases. It will be an important parameter of our simulation. The interesting temperature range is in the interval [0, 2], see Figure 15, which is of the order

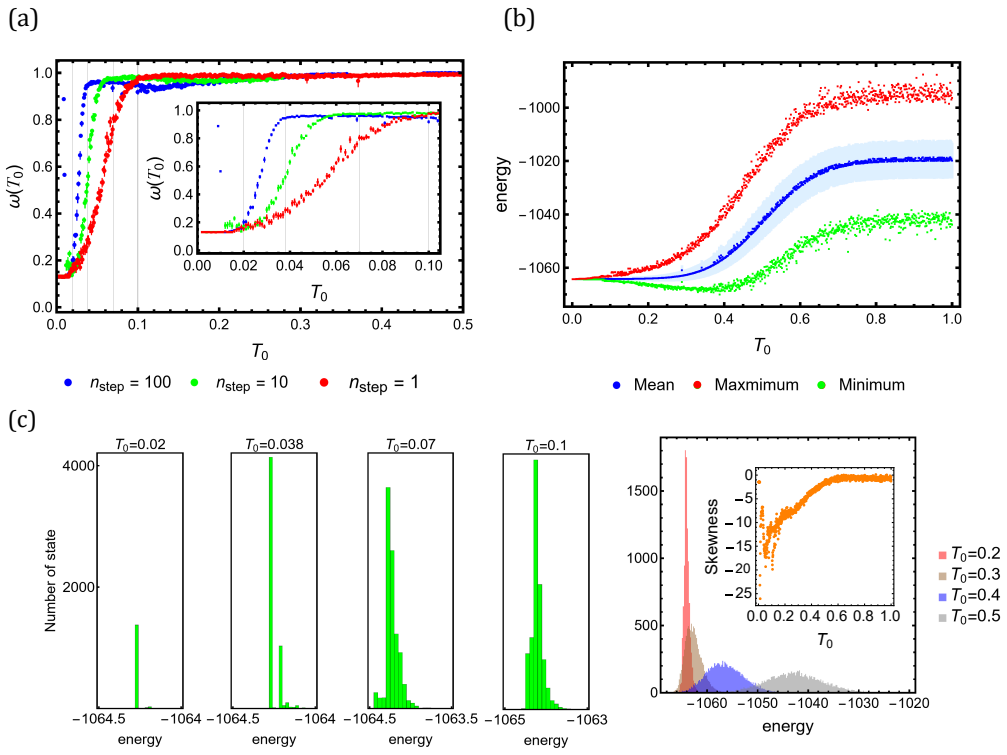

Figure 16: **(All)** Annealing and configurational space sampling: We chose a metastable state of size 30x30 characterized by low energy and conducted 10 000 simulated annealing runs. The simulations covered a range of T_0 values from 0.001 to 1, with increments of 0.001. **(a)** We plotted ω with standard deviation obtained by simulating the same scenario ten times. When $T_0 \to 0$, we found 1264 states with exactly the same energy. **(b)** For the simulation with $n_{step} = 10$, we plotted the mean, maximum, minimum, and standard deviation (*light blue*) of the energy for all simulations at each T_0 step. The standard deviation and the range of the distribution increase with T_0, as does the mean. **(c)** Histogram of the distribution of energy for different T_0 and $n_{step} = 10$, and the skewness. The probability of losing energy is always higher than that of gaining energy.

of the characteristic energy of spinner-spinner interaction. Finally, we will be able to start from an initial state and explore the neighbouring energetic landscape with temperature T_0 as a parameter to control the energy barriers that we may encounter.

Once we have a set of states found by simulated annealing, we will pose some questions: What is the distribution of a given distance between all pairs of states? How far is this set from ultrametricity? To perform this, we have implemented a clustering algorithm that deduces an ultrametric distance from a given distance. This algorithm works with single, complete, or average linkage. Naturally, the first study will be one on the influence of initial temperature in annealing simulation.

8 Influence of initial temperature

We have a functional simulated annealing algorithm that allows us to explore the energetic landscape of the spinner lattice. The main parameter is the initial temperature T_0, so we will study its influence by examining a set of metastable states found by annealing at a given T_0.

8.1 Energetic landscape exploration

First, we will address the question: What is the energy distribution of states found by simulated annealing at T_0? We will begin with an initial metastable state of size 30 by 30. We will conduct 10 000 annealing runs for a range of T_0 values from 0.001 to 1 in steps of 0.001. In addition, we have $\lambda = 0.95$, $T_f = 0.00001$ and $n_{\text{step}} = 10$.

Only a part of the 10 000 performed simulations leads to different states. We computed $\omega(T_0)$, which represents the fraction of different metastable states found (N_{found}) over $N_{\text{sim}} = 10000$ simulations at T_0 ($\omega = \omega_{\text{found}}/N_{\text{sim}}$). This is illustrated in Figure 16(a). The behaviour of ω is similar to what is observed in [41] and aligns with our expectations: for high T_0, we cross energetic barriers and find a plethora of different states, while for low T_0, we are unable to cross the energetic barriers from which we started. Additionally, we have studied the impact of n_{step} and have shown that an increase of n_{step} leads to a decrease in T where saturation occurs. Furthermore, the longer an annealing process is, the more time we have to find states, as it is related to the annealing of glassy solid matter, where the relaxation time is crucial for crossing energetic barriers. Additionally, the last observation is that as the limit $T_0 \to 0$ is approached, a second plateau occurs, indicating a large basin of energetically similar states, which is a first indicator of SG behaviour.

The parameter ω provides insight into the size of energetically accessible basins for a given T_0, but what is the distribution of energy ranges we have found? We will focus on simulations with $n_{\text{step}} = 10$ and compute the maximum, minimum, mean, and standard deviation of the energy distribution, as shown in Figure 16(b). We found the initial state by a very slow and high-temperature annealing, so we start from the bottom of a deep energy minimum. As T_0 increases, we can cross energetic barriers and find lower energy states. Additionally, this leads to an increase in annealing time, allowing us to move from one energetic minimum to a higher one. When examining the histogram of the energy distribution in Figure 16(c), we note a transition from a delta function to a Gaussian-like distribution. This transition leads to a flattening of the distribution as T_0 increases. This is indicated by the increasing standard deviation. Additionally, the kurtosis in the range [30,75] decreases, which is nearly an order of magnitude larger than that for a Gaussian distribution (i.e. 3). This can be explained by the increase in annealing time, which means more random changes and thus more opportunities to gain or lose energy. When this probability becomes equal, the distribution becomes symmetric, see Figure 16(c) and the skewness. A connection can be made with the concept of straggling in nuclear physics [59], where ions gain and lose energy through random collisions. Finally, above $T_0 = 0.7$, the distribution no longer changes, which can be attributed to the finite size of the lattice. We have performed the same study with the states having the lowest and highest energy and observed that the minimum of the mean does not appear for the lowest, while for the highest, it maintains the same depth as the total energy range for all T_0.

We know the T_0-dependence of the energy of the state found by simulated annealing. But remains the question of the disposition of this state in the configurational space: there are uniformly disposed? there are clusters? it is distance-dependence?

8.2 Configurational space exploration

We have seen that the energetic landscape has a large number of local minima and a first instance of the possibility of minimum similar basins in figure 16(b). We will study the disposition of metastable states on the configurational space; remember that this is only a small fraction of the points of Ω that are metastable.

We will use the four distances defined previously: Ha, IHa, GE and LE, see Eqs.(6.2-6.5), and compute all distances two-by-two states on the set generated in section 8.1. What is the distribution? This is an important question because it can be related to order parameters for SG [7], as well as the notion of hierarchical energetic landscape and RSB. The maximum, the minimum, the mean, and the standard deviation of these

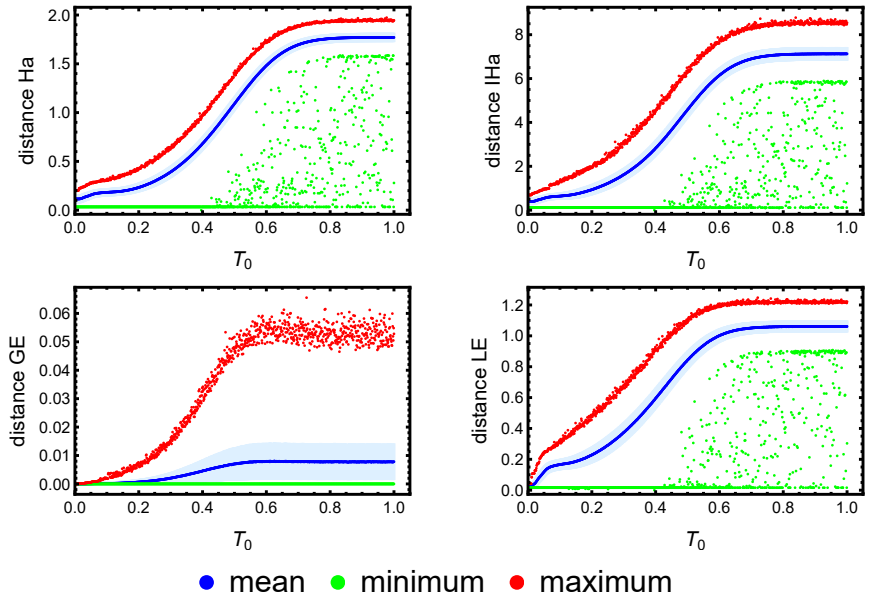

Figure 17: **(All)** The mean, minimum, and maximum distances between two different states were computed over a set ranging from 1264 to 10000 states, obtained through annealing of an initial 30 by 30 lattice (see Figure 29). Thus, the statistics are based on a set with a cardinality ranging from 1 596 432 to 99 990 000 for each T_0 value. This statistical analysis is performed on the simulations presented in Figure 16. The *light blue* colour represents the standard deviation. **(bottom-right)** We can note a more pronounced step-function behaviour near $T_0 \approx 0.07$ than for the top plot

four distributions are shown in Figure 17. In all plots, we observe that above approximately $T_0 \approx 0.7$, the mean and maximum curves flatten out. This could indicate that an increase in temperature does not affect configurational space sampling, suggesting that we are in a random walk regime. Additionally, the increase before $T_0 \approx 0.7$ can be attributed to a significant augmentation of the probability of accepting unfavourable changes. This conclusion is supported by the similar behaviour of energy distribution, as depicted in Figure 16(b). For the distances Ha, IHa, and LE, the standard deviation remains relatively constant and low compared to the mean. This indicates that the states are relatively equidistant. As T_0 increases, the states become further apart. Additionally, differences in the minimum value can be attributed to variations in the speed and duration of the annealing process. In contrast, for GE, we notice that the mean is much closer to the minimum value than to the maximum value. This suggests a negative skewness in this distribution. Furthermore, in this scenario, the standard deviation also increases, likely due to the temperature increment.

Now we will focus on the skewness and kurtosis of distance distribution. These curves are plotted in Figure 18 and these values are significant as they will be compared with the order of standard deviation displayed in Figure 17. The interesting observation is the oscillations in all curves except for the GE distance, before becoming flat above a critical temperature of ≈ 0.7. What could explain these oscillations? The increase in T_0 leads to both longer annealing times and a higher probability of crossing energetic barriers. The increase in the Boltzmann factor increases asymmetry, meaning that values higher than the mean are better represented in the distribution, as the simulation explores further regions in the configurational space. However, it appears that simulations can leave energetic minima that are induced by the increase in annealing time leading to a decrease in asymmetry. It seems that simulations have more time to reach an energetic minimum. In addition, the asymptotic behaviour of skewness is interesting. For Ha, it is positive; nearly null for LE; and equal and negative for GE and IHa. For the kurtosis, we can note that all curves, except for GE, converge to 3, which is the kurtosis of a normal distribution. It appears that the LE and IHa curves exhibit

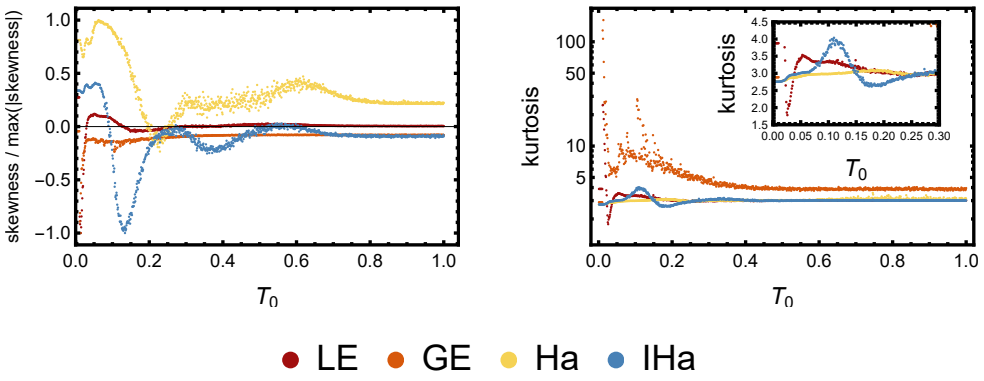

Figure 18: **(Left)** Evolution of skewness, as defined in Eq.(B.3), as a function of T_0. The values are normalized by the absolute maximum skewness for LE, GE, Ha, and IHa distances, which are respectively 3.13, 12.66, 0.2485, and 0.599. **(Right)**We have plotted the kurtosis for all distances, as defined in Eq.(B.4).

similar behaviour to skewness. Furthermore, the Ha curve demonstrates relatively flat behaviour across the entire range of T_0. The distinction between Ha and IHa is significant despite their closely related definitions.

The question remains: do we have unimodal or multimodal distributions? This is an important question to highlight the presence of clusters in the configurational space. The answer lies solely in examining the histograms of the distribution, as depicted in Figure 19. We have confirmed that for a high T_0, the distribution is unimodal and normal. However, below $T_0 = 0.25$, the LE distance distribution is multimodal. What happens? As T_0 approaches 0, the distribution becomes unimodal, indicating that we encounter states with very similar energy densities. As T_0 increases, the number of modes in the distribution increases until they merge into a Gaussian distribution. This phenomenon can be explained by a cardinality of the set that is too low to capture all the peaks on the histogram. Additionally, the main mode increases with temperature. Multimodality is a significant result. What does this mean? The multimodal behaviour of the distance distribution implies the existence of clusters of metastable states. For GE, we did not observe clusters, but we did for LE. Additionally, while we observed multimodality for Ha, it appeared less smooth compared to LE. Some empty bins in the histogram indicate that certain combinations of angles for the spinner are not available. The absence of certain combinations in the histogram for Ha could be related to the presence of the C_6 axis of the hexagonal cell because they are not empty bins for IHa, a distance invariant under C_6. This axis implies specific symmetry constraints on the orientations of the spinner, leading to certain combinations being forbidden or less likely in the dataset.

The large number of states with the same energy and the multimodality of distribution are both clues to indicate a hierarchy in the energetic landscape. The next step is the measurement of the degree of ultrametricity of this distribution. It can help to know if the experimental setup is a spin glass.

8.3 Ultrametricity of sampled set

One question we aim to answer is whether the configurational space is UM or not. Naturally, we will begin by studying how far from ultrameticity the set we have generated in section 8.1 is. We have plotted the degree of UM for the four distances in Figure 20.

We can see that below $T_0 = 0.25$, the GE curve increases consequently to broadening of energetic distribution, see Figure 16. In addition, the minimum point of the LE curve coincides with the temperature at which the distance distribution exhibits the maximum number of modes, and these modes have not yet

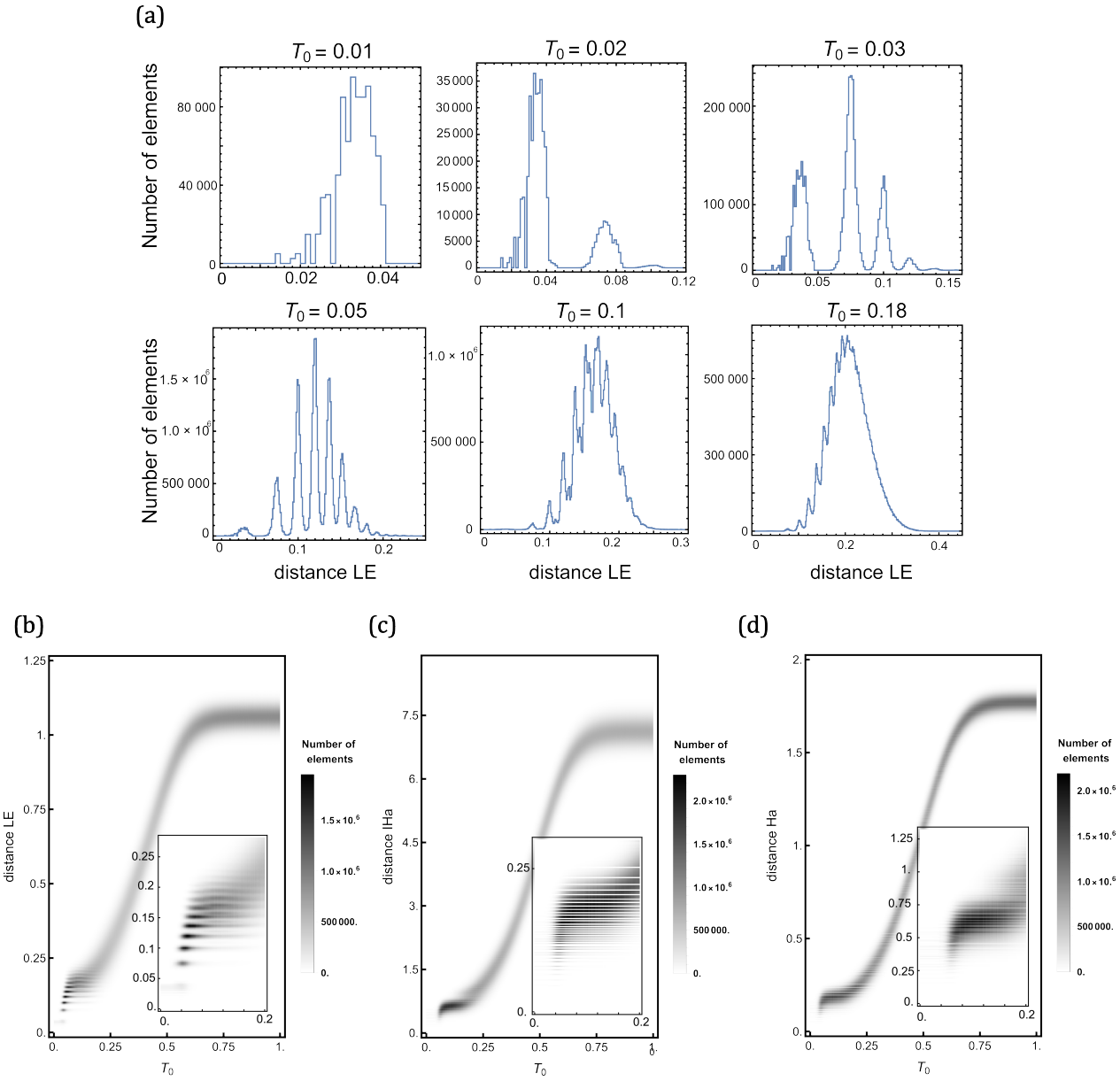

Figure 19: **(All)** All histograms have been constructed using one thousand bins of equal size over distance value ranges of [0, 1.25], [0, 2], and [0, 8.8] for LE, Ha, and IHa, respectively. These distance values are computed from the simulation described in Figure 8. **(a)** Histogram of distance LE distance for diffrente value of T_0.Successively, the distribution transitions from multimodal to unimodal, resembling a normal distribution. As T_0 increases, the highest mode shifts to larger values. Additionally, we observe that the shape of the top-left histogram is recovered at the right side of the top-middle and top-right histograms. **(b-d)** Each vertical line of pixels represents a histogram with a color code. Therefore, we have represented a histogram for a thousand values of T_0. **(b)** We can observe the transition from a multimodal distribution to an unimodal one. Additionally, the smaller the distance, the closer the modes are to each other, eventually reaching a continuous limit. **(c)** The distribution is sharper than that of LE, with noticeable distinct empty bands. **(d)** The main difference with Ha is that the distribution is smoother.

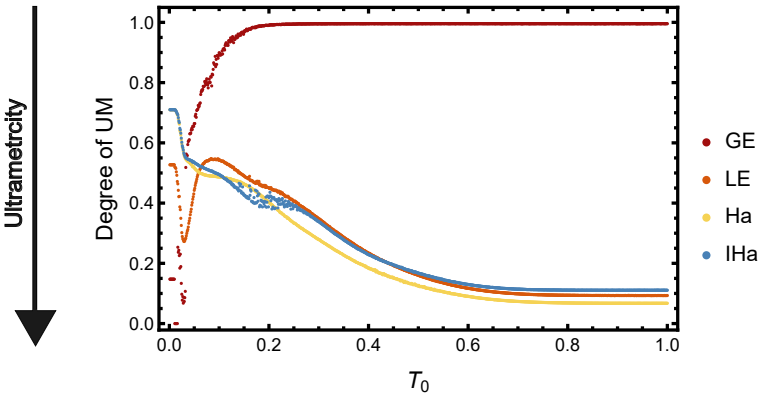

Figure 20: We compute the degree of UM as a function of T_0 for all considered distances, based on the set depicted in Figure 16. A vanishing degree indicates perfect ultrametricity. The asymptomatic behaviour of LE, Ha, and IHa distance correspond to perfect ultrametricity. But the interesting thing is what happens before par instance the local minima of LE curve.

overlapped with a Gaussian distribution. Above $T_0 = 0.25$, the degree decreases. This occurs when the distance distribution converges towards a Gaussian distribution, as shown in Figure 18. (right), and when the mean distance significantly increases, as seen in Figure 17. Consequently, the degree of UM decreases because the ratio of mean to standard deviation increases. Indeed, all elements become equidistant in the asymptotic behaviour: it's a trivial example of UM set. Furthermore, above $T_0 = 0.6$, the curve flattens out because the distribution does not change anymore. We have now a good insight into the influence of T_0 on the simulated annealing algorithm implemented to find metastable spinners configuration.

8.4 Summary

We conducted a complete study of the influence of T_0. We demonstrated the broadening of the energy distribution as T_0 increases and observed significant variations in $\omega(T_0)$. We have found numerous states with the same energy. Furthermore, we highlighted the importance of skewness and kurtosis in explaining and describing the behaviour of the distribution. When annealing is capable of crossing energetic barriers, we can observe the effect in the skewness.

After studying the disposition of metastable states in the configurational space using specific distances, we demonstrated that for a given T_0, all states are equidistant with a slight correction as a normal distribution. Furthermore, we showed that at low temperatures, we can observe a multimodal distribution, which is a significant indicator of the cluster structure of metastable states, especially for LE.

Finally, we conclude that the method of sampling the configuration space is crucial in determining the degree of UM, which is consequently strongly dependent on T_0. To study the influence of the number of spinners and the lattice parameter on the degree on UM, we will design an annealing method able to sample a representative region on the configurational space. It will be done in the following section.

9 Thermodynamic limit

The essence of SG phase is the the breaking of replicas symmetry where there a lots a metstable configuration that can be sort as an UM tree [60]. Consequently, the first question that often arises in the literature [58, 60] and generally in statistical physics is: what happens when the number of elements tends to infinity? How does the system behave in the thermodynamic limit? In this section, we will examine the impact of the

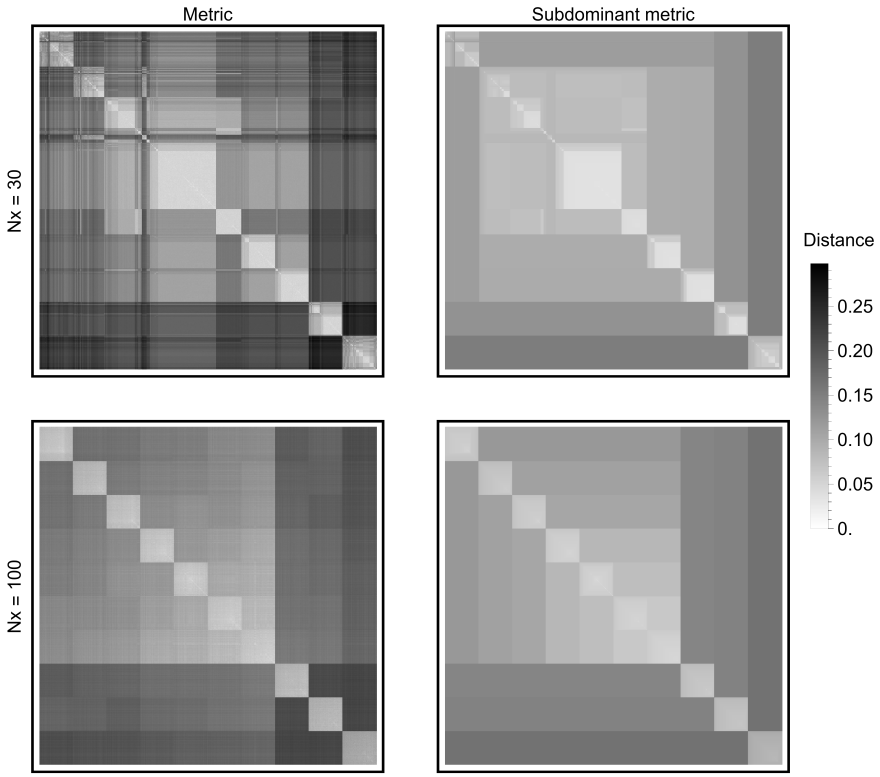

Figure 21: **(All)** Distance matrix for LE distance: The results are analogous to those found in the literature for Spin glass (SG) [60, 61]. Note that the rows and columns are sorted by Euclidean distance. This is a 1279×1279 matrix. **(Left)** This is the metric distance matrix for LE. **(Right)** This is the subdominant metric derived from the original metric using a clustering algorithm that employs single-link dissimilarity.

number of spinners on the degree of UM.

9.1 Method

We need to design a method to sample the configurational space of systems with various N. We have observed that simulated annealing can effectively explore and sample the vicinity of an initial state for $T_0 < 0.2$, as shown in Figure 19(b-d). However, for higher T_0, the distance distribution becomes unimodal, indicating that the states found are equidistant. This is a consequence of the process used and not an intrinsic property of the system.

To sample both the neighbouring configurational space and the entire configurational space, we need a process that accounts for varying annealing temperatures and a wide range of configurations. Here's a three-step method to achieve this:

1. Choose an initial metastable state with both a low and high initial annealing temperature.

2. Perform ten annealings with a random T_0 uniformly chosen in the range $[0.04, T_{\max}]$, with $\lambda = 0.95$, $n_{\text{step}} = 10$, and $T_f = 0.00001$.

3. Based on the ten resulting states, perform 10×128 annealings with $T_0 = 0.04$, $\lambda = 0.1$, $n_{\text{step}} = 10$, and

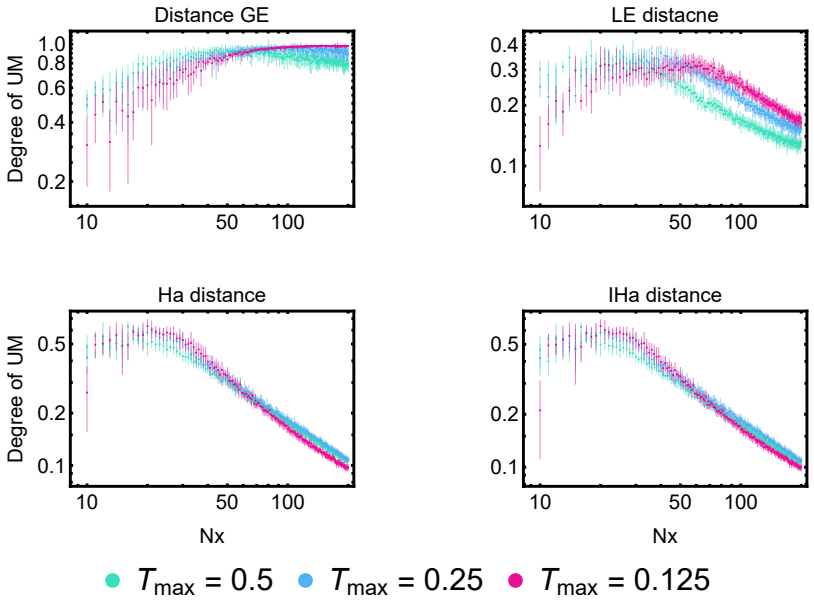

Figure 22: Degree of Ultrametric (UM) for the four considered distances. Three values for $T_{\max}$ were considered to study the influence of this parameter. The average is over ten simulations.

$T_f = 0.00001$.

By combining these steps, the method allows for both broad sampling across a range of configurations and detailed sampling of local metastable states. The variable temperatures in step 2 ensure diversity in the initial sampling, while the focused sampling in step 3 allows for in-depth exploration of the local configurational space. Plus, we have decresae λ in order to incresse $\omega(T_0)$. Finally, to ensure robust results, we will average over ten different simulations.

An example of a generated set is shown in Figure 21. We need to select an initial state with 30×30 spinners and another with 100×100 spinners, and then apply our annealing method. Using the set of metastable configurations we find, we can calculate a distance matrix using the metric known as LE distance. Subsequently, by using a clustering algorithm that employs single linkage, we can compute the subdominant metric distance. If both the distance matrices, metric and subdominant, are the same, then we have a perfect ultrametric set.

9.2 Results

We will compute the degree of UM for a range of N_X, the root square of the number of spinners, from 10 to 200. Plus, we will make an average of over ten simulations and we have considered three different $T_{\max}$. The results are displayed in Figure 22. Clearly for LE, IHa and Ha distance the degree of UM vanish in the thermodynamic limit with approximatively the scaling $\sim N_X^{-1}$ or $N^{-0.5}$. This decrease occurs after $N_X = 50$, 20 and 20, respectively. Before this, there is either an increase or a plateau, which can be attributed to finite-size effects. This influence of size is rarely explored in the literature [49].

Thus, we can conclude about the asymptotic UM behaviour of the configurational space. Moreover, there seems to be independence of the asymptotic results for different $T_{\max}$ values. Conversely, for the GE distance, the asymptotic behaviour suggests a completely non-UM set. Plus, we can change another parameter as the lattice parameter, and it can be have an interesting effect of the set found.

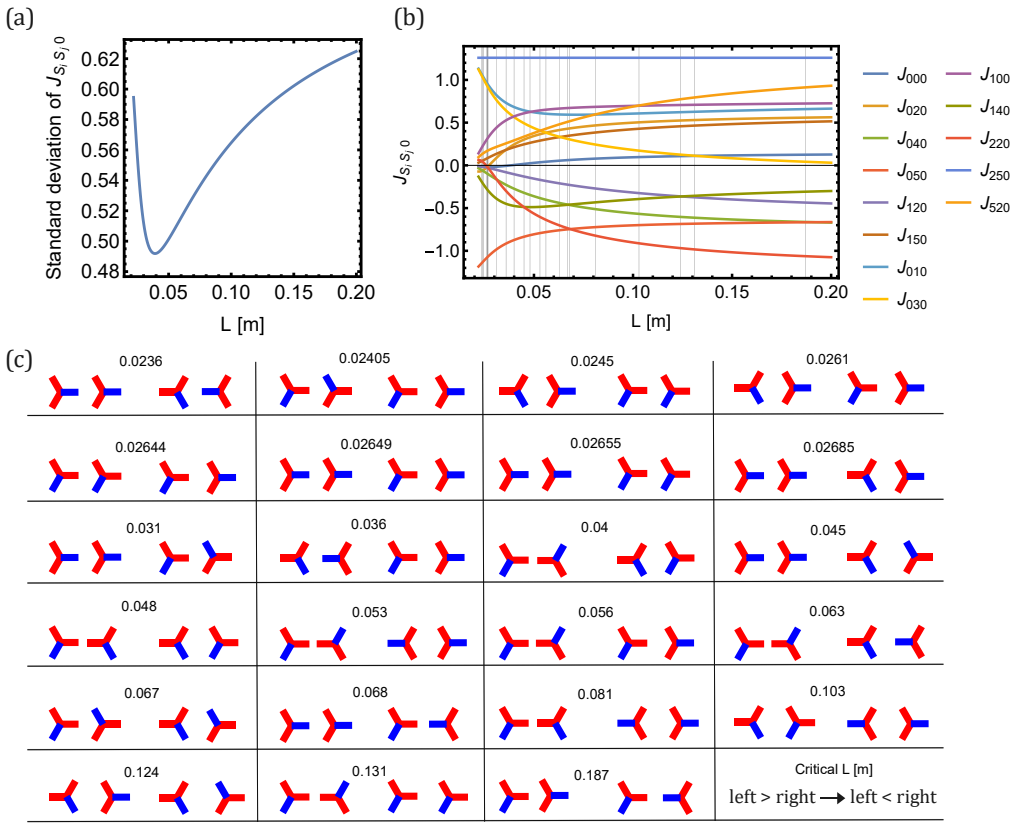

Figure 23: **(Top-Left)** Standard deviation of the 13 different elements in the tensor $J_{S_i S_j k_{ij}}$. **(Top-Right)** The L-dependence of the 13 different elements in the tensor $J_{S_i S_j k_{ij}}$. The vertical curve indicates the critical value of L where two elements of $J_{S_i S_j k_{ij}}$ are equal. **(Bottom)** Explicit representation of each critical L where two element of $J_{S_i S_j k_{ij}}$ become equal. Each case corresponds to a vertical curve of **Top-Right**. The bottom-right diagram shows the convention used: the critical value of L is expressed in meters. Below this critical value, the left interaction is stronger than the right interaction. Above this value, the reverse is true, with the right interaction being stronger than the left interaction.

10 Influence of L

Besides the number of spins, the second key parameter that can impact the UM of the configuration space is the lattice parameter. We will explore how this parameter influences the interaction tensor and the ultrametricity of the set of metastable states.

10.1 L dependence of the interaction tensor

The elements of the tensor $J_{S_i S_j k_{ij}}$ are constructed as the sum of nine dipole-dipole interactions, see Eq.(3.1). We can expect these interactions to scale approximately as $\sim L^{-3}$. Despite this scaling, it is the relative importance of the elements concerning each other that matters, rather than their absolute values. This is because the energetic landscape would still exhibit the same minima even if the entire energy scale is multiplied by a constant. To create a consistent method across a wide range of L, we will normalize all elements so that the largest one has a constant value of 1.25891, which corresponds to the element J_{250}. The advantage of this strategy is that it maintains a constant order for $\Delta E/T$. The L-dependence of $J_{S_i S_j k_{ij}}$, along with the critical value of L at which two different elements become equal, is displayed in Figure 23. We will study the distance distribution over a set of metastable states for a range of lattice parameters.

10.2 Study of a restricted region of energetic landscape

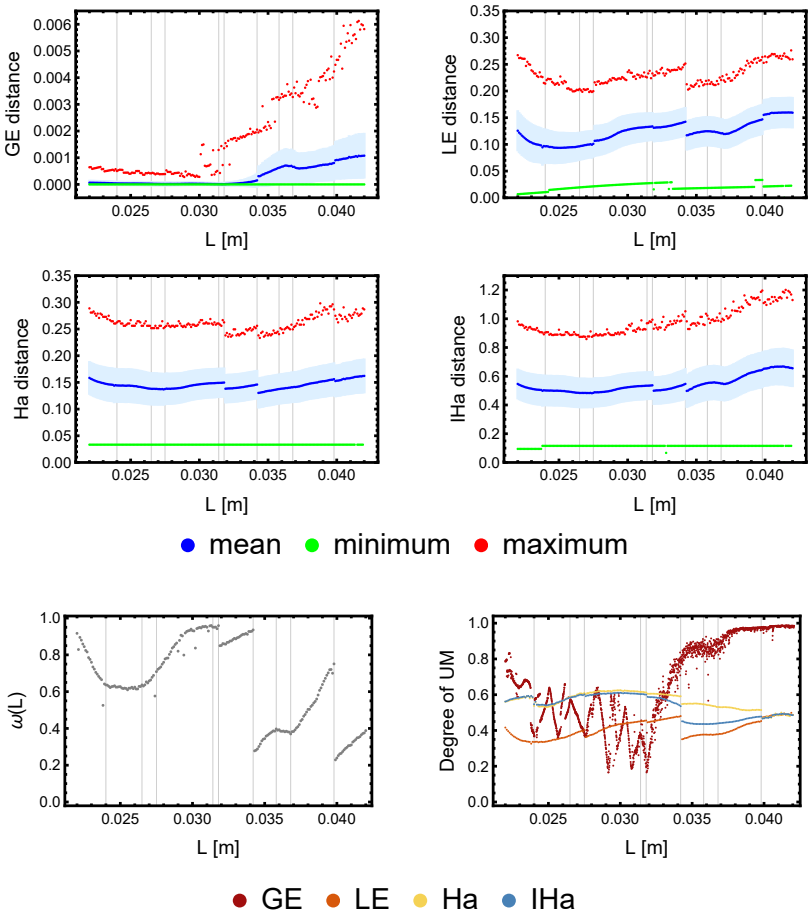

Figure 24: **(All)**One thousand simulated annealing runs were performed on the initial 30 by 30 state shown in Figure 29, with parameters set to $\lambda = 0.95$, $n_{\text{step}} = 10$, $T_f = 0.00001$, and $T_0 = 0.04$. The vertical lines serve as visual guides to aid in the comparison between graphs. **(Top and Middle)** We plotted the maximum, minimum, mean, and standard deviation for the distribution of the four considered distances. **(Bottom-Left)** We observe some jumps of parameter $\omega(L) = N_{\text{found}}/N_{\text{sim}}$. **(Bottom-Right)**This represents the degree of UM for all distances. There are some oscillations observed for GE.

We have noticed that the relative importance of the elements in the interaction tensor varies greatly with the lattice parameter L. Now, we will investigate how this impacts the configuration space when constrained to a quasi-constant energetic hypersurface. To achieve this, we have conducted a low-temperature annealing process on a 30×30 initial state. We perform one thousand simulations on the initial 30 by 30 state, shown in Figure 29, with $\lambda = 0.95$, $n_{\text{step}} = 10$, $T_f = 0.00001$, and $T_0 = 0.04$. The results are displayed in Figure 24.

In Figure 24 (top-middle), the first observation is that the extreme jumps or oscillations do not correspond to points where two different elements of the interaction tensor become equal or to a critical value of L. The first insight comes from the GE plot, where we can distinctly observe two jumps for the maximum value. The magnitude of the jump, Δd^N_{GE}, corresponds to a distance where an alignment of two dipoles is created. As L increases, it becomes easier to create this alignment, which can be attributed to a decrease in the standard deviation of the tensor elements, see Figure 23(a). This implies that the relative depth of a minimum

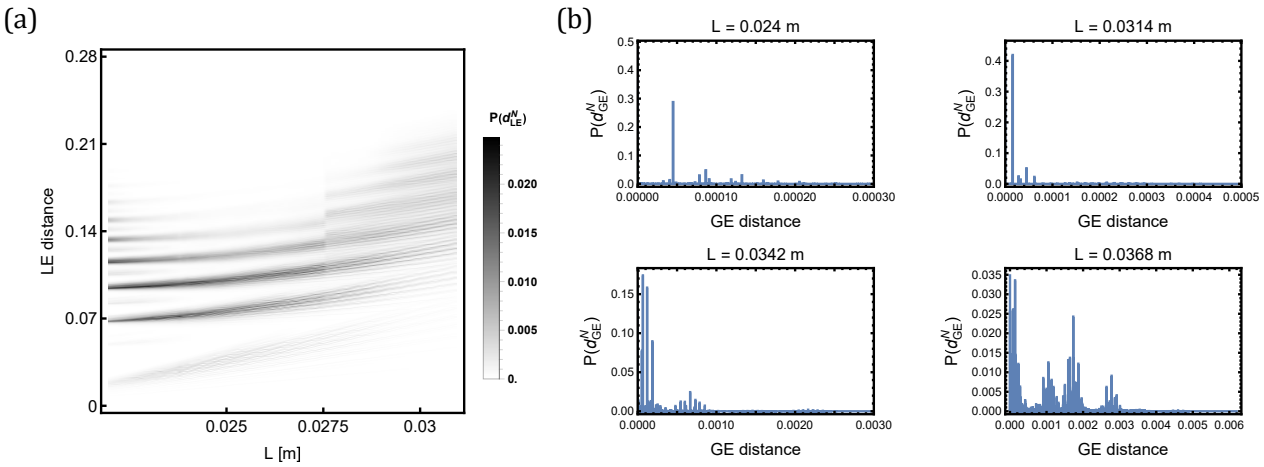

Figure 25: **(All)** The function $P(d_X^N)$ represents the probability of finding the distance d_X^N within a given histogram. This enables the use of a single colour code across multiple histograms, even when they contain different numbers of states. **(a)** This histogram has 1000 bins spanning the range from 0 to 0.28. **(b)** This is some zoomed-in view of the histogram, with 10000 bins spanning the range from 0 to 0.0062, showing results for various distances L.

corresponding to alignment, compared to a minimum without alignment, becomes smaller as we increase L from 22 mm to 42 mm. The second observation is from the plot in Figure 24(bottom-left). The jump in parameter ω corresponds to the jumps in the mean or maximum values shown in the plot in Figure 24 (top-middle). This is a critical point: even a small variation in L can create or destroy many metastable states in the vicinity of the configuration space of the initial state.

How does this affect the degree of UM among neighbouring states? This is illustrated in Figure 24 (bottom-right). The curves for LE, Ha, and IHa show the same discontinuity observed in the distance distribution. It is interesting to note that the Hamming distance curves are superimposed over some ranges of L, but differ in others. Additionally, the GE curve reveals three distinct patterns: an oscillatory mode, a region with significant fluctuations, and a final segment with a nearly flat curve.

The last thing to examine is the histogram of the distance distribution. For Ha and IHa, the histograms don't reveal anything particularly remarkable, except for a limited number of peaks that roughly form a Gaussian shape. The density of these peaks tends to increase with distance. Consequently, we will focus on the histograms for LE and GE. These can be found in Figure 25. The LE plot is quite interesting: it shows a multimodal distribution, and as L increases, each mode splits into about ten distinct modes. What does this suggest? It could be a sign of a kRSB phase transitioning into a (k+1)RSB phase. The expansion of the lattice induces a significant change in the relative importance of elements within the interaction tensor, leading to a reorganization of the energy landscape. As L increases, this process results in the creation of additional sub-basins within pre-existing energy basins. Additionally, for the GE distance, we can compare the histogram with the plot in Figure 24 (bottom-right). In the range between about $L = 0.0240$ m and $L = 0.0314$ m, the curve exhibits oscillations. The reason for these oscillations is explained by the corresponding histograms: only a few bins are occupied, and as L increases, the bin ratio changes, leading to the oscillatory behaviour. The peaks in the oscillation curve correspond to changes in the bin ratio due to changes in the interaction tensor. Moreover, this occurs just before annealing can create additional alignment of two dipoles, as shown in Figure 24 (top-left). Additionally, the region with a lot of fluctuations between $L = 0.0342$ m and $L = 0.0368$ corresponds to the area in Figure 24 (top-left) where there are some discontinuities. Above this range, there's a multimodal distribution with a very low characteristic of UM. However, we have only focused on

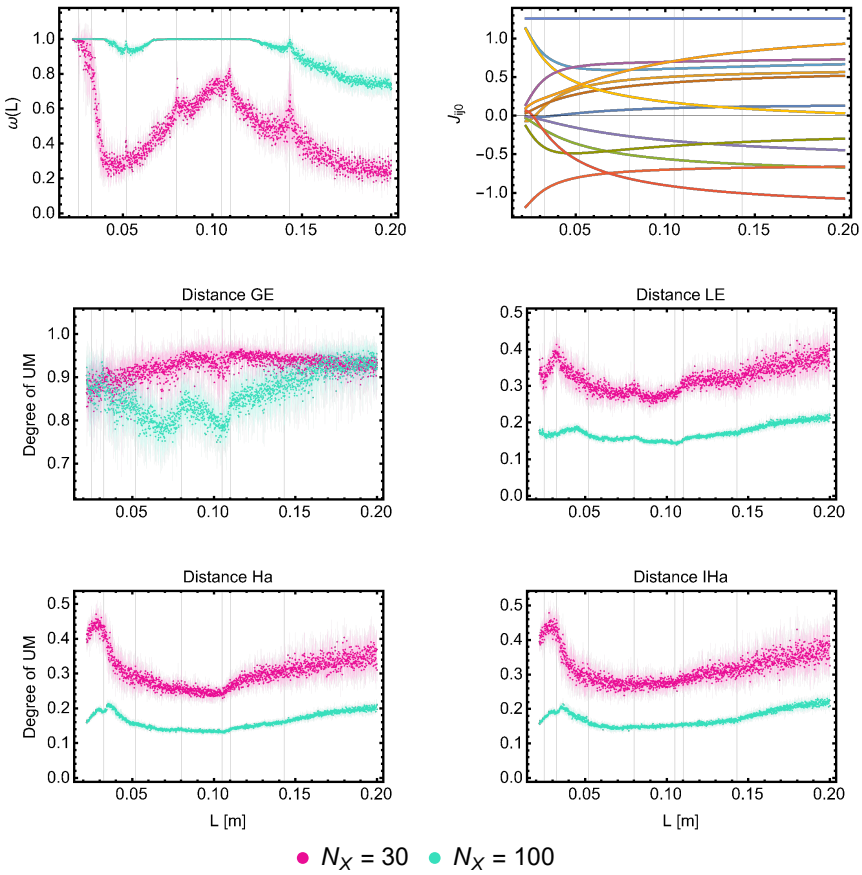

Figure 26: **(All)** The vertical line serves as a guide to help compare all the plots. **(Top-Left)** The ω curve shows distinct peaks for specific values of L. **(Top-Right)** The L-dependence of the elements of the interaction tensor. **(Middle-Left)** The are a remarkable intersection between curve for $N_X = 30$ and $N_X = 100$. **(Middle-Right and Bottom)** The tree plot have a similar behaviour.

the hypersurface of quasi-constant energy in the configurational space. The next step is to explore all the configurational space.

10.3 L dependence for the degree of UM

After exploring a quasi-constant energetic hypersurface of the configuration space, our focus shifts to examining the behaviour across the entire configuration space. We will follow the same procedure described in Section 9.1, but this time we will change L instead of N. What is the L-dependence of the degree of UM?

In Section 10.1, we established that the elements of the interaction tensor exhibit complex behaviour as L changes. Additionally, Section 10.2 indicated that both the degree of UM and the parameter ω have a strong dependence on L. We have performed a degree of UM for a range of lattice parameters and two sizes of lattice, 900 and 10 000 spinners. Plus, we have made an average of over ten simulations. The results from the simulations are displayed in Figure 26. Here are some interesting observations. First, ω displays peaks for specific values of L, which do not depend on the system size. This suggests that the number of metastable states in regions of the configuration space accessible via the annealing process can be significantly higher for some specific values of L. Second, the degree of UM does not change in terms of magnitude over the broad range of L studied, unlike what is observed in studies approaching the thermodynamic limit. Nevertheless,

for the Ha, IHa, and LE curves, we observe a maximum around $L = 0.03$ m when $N_X = 30$. However, for $N_X = 100$, the peak corresponds to a higher value of L. This observation is significant, as it suggests that the dependence on L and the size effect are coupled.

We can conclude that the degree of UM does not vanish as L tends to infinity; instead, it varies with L, but the order of magnitude remains constant. Additionally, we note that the parameter ω has a strong dependence on L and that the effects of L and N are interconnected.

10.4 Summary

The increase of the lattice parameter L leads to significant reorganization of elements within the interaction tensor. This parameter impacts deeply the degree of UM, the distance distribution and the parameter $\omega = N_{\text{found}}/N_{\text{sim}}$. At the level of the neighbourhood of the initial state in the configurational space, we observed that only the GE and LE distances change significantly with L. Examination of the distance histogram has revealed potential evidence of a kRSB transition for the LE distance. Additionally, the histogram for the GE distance indicates that the energetic landscape contains different basins, distinguished only by the alignment of two dipoles, with each sub-basin representing states with the same number of alignments. Furthermore, the study of the degree of UM across the entire configuration space has revealed the presence of both a peak and a minimum.

Part IV

Conclusion

The objective of this thesis was to propose an experimental model for a spin glass based on "spinners," which are made up of point dipoles surrounding a ball bearing. This is a gap in the study of spin glass. We utilized numerical simulations to determine whether our setup exhibits the complexity, energy degeneracy, and ultrametric energetic landscape characteristic of spin glass.

First, after making experimental observations, we have chosen to consider a discrete model because its simplicity was useful for performing numerical simulations. We need to define a spin glass Hamiltonian that respects the symmetry and anisotropy of our arrays of spinners. The first result in Section 4.2 has shown that the number of metastable states decreases as the lattice parameter and the external magnetic field increase. When the number of states scales as 6^N, the count of metastable states scales as $6^{0.522N}$.

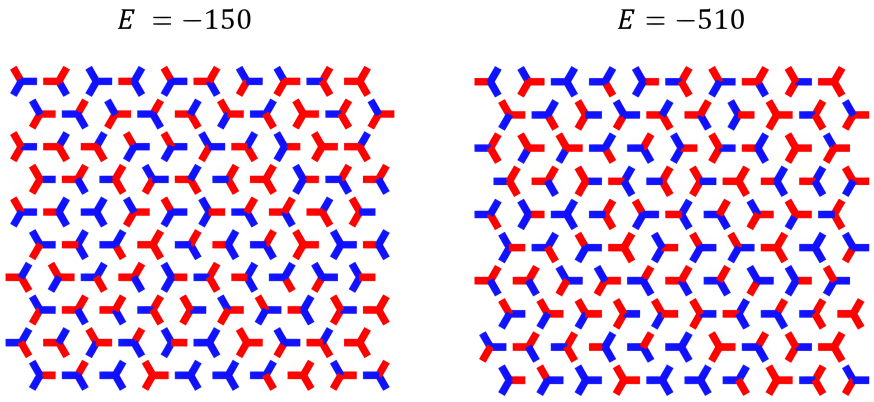

Figure 27: Two arrays of spinners 10×10 that look similar at first sight but their energy is different by a factor of 3.4.

In Section 8, we conducted a thorough study of the impact of T_0 on our annealing simulation. We observed that as T_0 increases, the energy distribution broadens, and we noted significant variations in $\omega(T_0) = N_{\text{found}}/N_{\text{sim}}$. We also identified several states with the same energy, indicating that our system exhibits characteristics of a spin glass. Additionally, by examining the arrangement of metastable states in the configuration space using specific distances defined in Section 6 based on Hamming and energy distance, we showed that for a given T_0, all states are equidistant with a slight correction resembling a normal distribution. Furthermore, we demonstrated that at low temperatures, a multimodal distribution can be observed, which is a key indicator of the cluster structure of metastable states, especially for LE. Another indicator is the oscillatory behavior of kurtosis and skewness in the distance distribution. Plus, the degree of UM is strongly dependent on T_0.

What happens in the thermodynamic limit? We studied an array ranging from 100 to 40 000 spinners in Section 9. After devising a method in Section 9.1, we seen that the degree of ultrametricity vanished for Ha, IHa, and LE distance in the thermodynamic limit. This indicates that the configurational space and the energetic landscape become ultrametric. However, the configurational space did not become ultrametric for the GE distance.

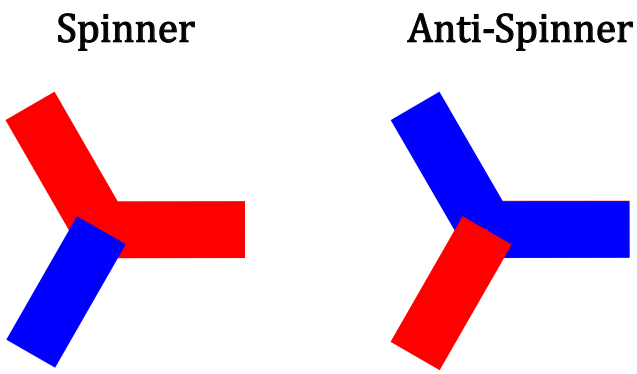

Figure 28: Representation of a spinner and an anti-spinner. Blue corresponds to inward dipole, and red corresponds to outward dipole.

We have conducted a study on the influence of the lattice parameter as it controls the Hamiltonian of our system. This parameter has a significant impact on the degree of UM, the distance distribution, and the parameter $\omega(L) = N_{\text{found}}/N_{\text{sim}}$. Analysis of the distance histogram, over a set of metastable state generate by low temperature anneling, has revealed potential evidence of a kRSB transition for the LE distance. Furthermore, the histogram for the GE distance suggests that the energetic landscape contains different basins, distinguished only by the alignment of two dipoles, with each sub-basin representing states with the same number of alignments. In our analysis of the entire configuration space, we have discovered both a peak and a minimum in the degree of UM.

In conclusion, we have presented evidence, such as ultrametricity and the numerous degeneracy of an energy level, indicating that the experimental model exhibits spin glass behaviour and can function as a macroscopic device for studying and explaining the behaviour of glass materials. Specifically, this is an original way to study replica symmetry breaking and the ultrametric structure of an energetic landscape. The structure of a spinner can be modified to study other behaviours or parameters such as correlations.

To go further, we could explore a continuous version to better align with the experimental setup. Additionally, we can implement second neighbour interactions or consider that the dipole has a finite size rather than being a point dipole. It might be worthwhile to investigate other lattices such as the Kagome lattice. Furthermore, the number of dipoles per spinner can be adjusted. Plus, study a LE distance with a C_6 invariance like IHa will help to understand the importance of symmetry.

Another perspective to consider is the study of new parameters, such as the correlation length and its fluctuations. We have noted that spinner configurations can exhibit vastly different energies while appearing similar at first glance. This phenomenon is depicted in Figure 27 by two examples of arrays. Developing a characteristic length that can explain this energy variation is a challenge analogous to some remaining questions on spin glass [7].

Finally, it will be very interesting to study a model involving spinners and anti-spinners. Anti-spinners are similar to spinners but with outward dipoles replaced by inward dipoles, and vice versa, as shown in Figure 28. The interaction tensor between spinner and anti-spinner is given by $\epsilon_{ij} J_{S_i S_j k_{ij}}$. Here, ϵ_{ij} is 1 if spinners i and j are both spinners or both anti-spinners, and ϵ_{ij} is -1 if one is a spinner and the other is an anti-spinner. It is a way to introduce an external random variable, similar to spin glass theoretical models: the distribution of anti and spinners. This will be analogous to the $\pm J$ spin glass model [7].

A Lattice of spinners

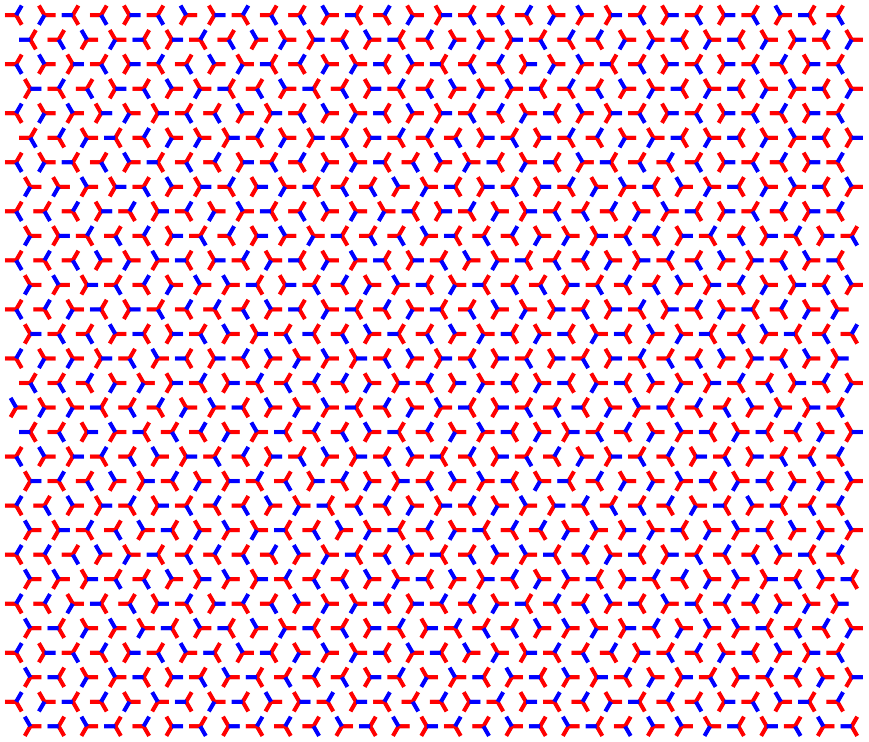

Figure 29: 30×30 metastable lattice

B Statistics moments

Lets consider a set $X = \{X_i : 1 \leq i \leq N\}$. The mean of X is given by

$$\mu = \mathbb{E}(X) = \frac{1}{N} \sum_i X_i, \tag{B.1}$$

the standard deviation by

$$\sigma = \sqrt{\mathbb{E}((X-\mu)^2)} = \sqrt{\frac{1}{N-1} \sum_i (X_i - \mu)^2}, \tag{B.2}$$

the skewness by

$$\mu_3 = \frac{\mathbb{E}((X-\mu)^3)}{\sigma^3} \tag{B.3}$$

and the kurtosis by

$$\mu_4 = \frac{\mathbb{E}((X-\mu)^4)}{\sigma^4}. \tag{B.4}$$

References

[1] M. C. Fuhs and D. S. Touretzky, *A spin glass model of path integration in rat medial entorhinal cortex*, J. Neurosci. **26**, 4266 (2006).

[2] A. G. Hudetz, C. J. Humphries, and J. R. Binder, *Spin-glass model predicts metastable brain states that diminish in anesthesia*, Front. Syst. Neurosci. **8**, 234 (2014).

[3] D. L. Stein, *Spin glasses and biology* (World Scientific Press New York, 1992).

[4] G. Biroli, G. Bunin, and C. Cammarota, *Marginally stable equilibria in critical ecosystems*, **20**, 083051 (2018).

[5] F. Shafee, *Spin-glass-like dynamics of social networks*, arXiv preprint physics/0506161 (2005).

[6] G. Parisi, P. Urbani, and F. Zamponi, *Theory of simple glasses: exact solutions in infinite dimensions* (Cambridge University Press, 2020).

[7] M. Mézard, G. Parisi, and M. A. Virasoro, *Spin glass theory and beyond: an introduction to the replica method and its applications*, Vol. 9 (World Scientific Publishing Company, 1987).

[8] G. Parisi, *Nobel lecture: multiple equilibria*, Rev. Mod. Phys. **95**, 030501 (2023).

[9] M. Müller and M. Wyart, *Marginal stability in structural, spin, and electron glasses*, Annu. Rev. Condens. Matter Phys. **6**, 177 (2015).

[10] P. Koželj, S. Vrtnik, M. Krnel, A. Jelen, D. Gačnik, M. Wencka, Z. Jagličić, A. Meden, G. Dražić, F. Danoix, et al., *Spin-glass magnetism of the non-equiatomic cocrfemnni high-entropy alloy*, J. Magn. Magn. Mater. **523**, 167579 (2021).

[11] R. Lauro-Grotto, *The unconscious as an ultrametric set*, Am. Imago **64**, 535 (2007).

[12] B. Dragovich and A. Y. Dragovich, *A p-adic model of dna sequence and genetic code*, P-ADIC NUMBERS ULTRA **1**, 34 (2009).

[13] A. Maiorano, G. Parisi, and D. Yllanes, *Ultrametricity and long-range correlations in the edwards-anderson spin glass*, dimension **36**, 40.

[14] R. Dennis and E. Corwin, *Jamming energy landscape is hierarchical and ultrametric*, Phys. Rev. Lett. **124**, 078002 (2020).

[15] R. H. Brill, *A note on the scientist's definition of glass*, J. Glass Stud., 127 (1962).

[16] J. Bicerano, *Glass transition*, EPST **2** (2002).

[17] C. A. Angell, *The glass transition*, Curr. Opin. Solid State Mater. Sci. **1**, 578 (1996).

[18] C. A. Angell and S. Sivarajan, *Glass transition*, JMST **4**, 3565 (2001).

[19] A. Cavagna, *Supercooled liquids for pedestrians*, Phys. Rep. **476**, 51 (2009).

[20] A. Einstein, *On the theory of the brownian movement*, Ann. Phys **19**, 371 (1906).

[21] J. H. Gibbs and E. A. DiMarzio, *Nature of the glass transition and the glassy state*, J. Chem. Phys. **28**, 373 (1958).

[22] J. Kurchan, *In and out of equilibrium*, Nature **433**, 222 (2005).

[23] S. S. Schoenholz, E. D. Cubuk, E. Kaxiras, and A. J. Liu, *Relationship between local structure and relaxation in out-of-equilibrium glassy systems*, PNAS **114**, 263 (2017).

[24] R. G. Palmer, *Broken ergodicity*, Adv. Phys. **31**, 669 (1982).

[25] P. W. Anderson, *Localisation theory and the cu-mn problem: spin glasses*, Mater. Res. Bull. **5**, 549 (1970).

[26] E. Ising, *Beitrag zur theorie des ferro-und paramagnetismus*, PhD thesis (Grefe & Tiedemann Hamburg, Germany, 1924).

[27] A. Kabelac, *One-and two-dimensional ising model*, (2021).

[28] G. Kotliar, P. Anderson, and D. L. Stein, *One-dimensional spin-glass model with long-range random interactions*, Phys. Rev. B **27**, 602 (1983).

[29] L. Onsager, *Crystal statistics. i. a two-dimensional model with an order-disorder transition*, Phys. Rev. **65**, 117 (1944).

[30] D. Sherrington, *Spin glasses: a perspective*, in *Spin glasses* (Springer, 2007), p. 45.

[31] S. Nagata, P. Keesom, and H. Harrison, *Low-dc-field susceptibility of cu mn spin glass*, Phys. Rev. B **19**, 1633 (1979).

[32] D. L. Stein and C. M. Newman, *Spin glasses and complexity*, Vol. 4 (Princeton University Press, 2013).

[33] M. Sarachik, E. Corenzwit, and L. Longinotti, *Resistivity of mo-nb and mo-re alloys containing 1% fe*, Phys. Rev. **135**, A1041 (1964).

[34] S. d. D. V. Volterra, F. Concetti, and G. Parisi, *The full replica symmetry breaking solution in mean field spin glass models*, (2019).

[35] S. F. Edwards and P. W. Anderson, *Theory of spin glasses*, Phys. F: Met. Phys. **5**, 965 (1975).

[36] E. Marinari, G. Parisi, F. R. Tersenghi, J. R. Lorenzo, and F. Zuliani, *Replica symmetry breaking in short range spin glasses: a review of the theoretical foundations and of the numerical evidence, to be published on j. stat*, Physics, cond-mat/9906076.

[37] D. Sherrington and S. Kirkpatrick, *Solvable model of a spin-glass*, Phys. Rev. Lett. **35**, 1792 (1975).

[38] S. Kirkpatrick, C. D. Gelatt Jr, and M. P. Vecchi, *Optimization by simulated annealing*, science **220**, 671 (1983).

[39] N. Metropolis, A. W. Rosenbluth, M. N. Rosenbluth, A. H. Teller, and E. Teller, *Equation of state calculations by fast computing machines*, J. Chem. Phys. **21**, 1087 (1953).

[40] L. H. Adams and E. D. Williamson, *The annealing of glass*, J. Frank. Inst. **190**, 597 (1920).

[41] E. K. Burke, E. K. Burke, G. Kendall, and G. Kendall, *Search methodologies: introductory tutorials in optimization and decision support techniques* (Springer, 2014).

[42] *Population par commune au 1er janvier 2023*, STATBEL.

[43] R. W. Hamming, *Error detecting and error correcting codes*, Bell Labs Tech. J. **29**, 147 (1950).

[44] M. Mohammadi-Kambs, K. Holz, M. M. Somoza, and A. Ott, *Hamming distance as a concept in dna molecular recognition*, ACS omega **2**, 1302 (2017).

[45] R. Rammal, G. Toulouse, and M. A. Virasoro, *Ultrametricity for physicists*, Mod. Phys. **58**, 765 (1986).

[46] B. Y. Wu, K.-M. Chao, and C. Y. Tang, *Approximation and exact algorithms for constructing minimum ultrametric trees from distance matrices*, J. Comb. Optim. **3**, 199 (1999).

[47] J. C. Gower and G. J. Ross, *Minimum spanning trees and single linkage cluster analysis*, J. R. Stat. Soc.C **18**, 54 (1969).

[48] R.Rammal, A. J.C. d'Auriac, and B. Douçot, *On the degree of ultrametricity*, J. Phys. Lett. **46**, 945 (1985).

[49] D. E. Pinto, D. M. Sussman, M. M. T. da Gama, and N. A. Araújo, *Hierarchical structure of the energy landscape in the voronoi model of dense tissue*, Phys. Rev. Res. **4**, 023187 (2022).

[50] P. Zerzucha and B. Walczak, *Concept of (dis) similarity in data analysis*, TrAC, Trends Anal. Chem. **38**, 116 (2012).

[51] D. Müllner, *Modern hierarchical, agglomerative clustering algorithms*, arXiv preprint arXiv:1109.2378 (2011).

[52] Z. Bar-Joseph, D. K. Gifford, and T. S. Jaakkola, *Fast optimal leaf ordering for hierarchical clustering*, Bioinformatics **17**, S22 (2001).

[53] P. Charbonneau, E. Marinari, G. Parisi, F. Ricci-tersenghi, G. Sicuro, F. Zamponi, and M. Mezard, *Spin glass theory and far beyond: replica symmetry breaking after 40 years* (World Scientific, 2023).

[54] H. A. Jahn and E. Teller, *Stability of polyatomic molecules in degenerate electronic states-i—orbital degeneracy*, Proc. R. Soc. Lond. A **161**, 220 (1937).

[55] J. Feret, *Groupes et espaces vectoriels*, (2017).

[56] P. Markstein, *The new ieee-754 standard for floating point arithmetic*, in Dagstuhl seminar proceedings (Schloss Dagstuhl-Leibniz-Zentrum für Informatik, 2008).

[57] I. P. Traversa-Tejero, *Estimation of the population of stars in the universe*, OALIB **8**, 1 (2021).

[58] A. Cacciuto, E. Marinari, and G. Parisi, *A numerical study of ultrametricity in finite-dimensional spin glasses*, Phys. A Math. Gen. **30**, L263 (1997).

[59] E. Bonderup and P. Hvelplund, *Stopping power and energy straggling for swift protons*, Phys. Rev. A **4**, 562 (1971).

[60] H. G. Katzgraber and A. K. Hartmann, *Ultrametricity and clustering of states in spin glasses: a one-dimensional view*, Phys. Rev. Lett. **102**, 037207 (2009).

[61] G. Hed, A. Young, and E. Domany, *Lack of ultrametricity in the low-temperature phase of three-dimensional ising spin glasses*, Phys. Rev. Lett. **92**, 157201 (2004).